FORSCHUNGSZENTRUM ROSSENDORF
Mitglied der Wissenschaftsgemeinschaft Gottfried Wilhelm Leibniz

WISSENSCHAFTLICH-TECHNISCHE BERICHTE
FZR-388
August 2003
ISSN 1437-322X

Krist`I Van Ouytsel

A Small Angle X-ray Scattering Method to investigate the crack tip in metals

Herausgeber:
Forschungszentrum Rossendorf e.V.
Postfach 51 01 19
D-01314 Dresden
Telefon +49 351 26 00
Telefax +49 351 2 69 04 61
http://www.fz-rossendorf.de/

Als Manuskript gedruckt

FORSCHUNGSZENTRUM ROSSENDORF
WISSENSCHAFTLICH-TECHNISCHE BERICHTE
FZR-388
August 2003

Krist`I Van Ouytsel

with assistance of Jürgen Böhmert and Gudrun Müller

A Small Angle X-ray Scattering Method to investigate the crack tip in metals

Final Report
of the Marie Curie individual fellowship project

Abstract

Structural materials, such as ferritic and austenitic steels or aluminium alloys used in the nuclear and aircraft industry, are subjected to external operational loads in different environments. Adopting a damage tolerant design principle, understanding the growth of preexisting or newly formed cracks under these conditions is of prime relevance to prevent extensive crack propagation and failure of the component.

Within this framework, the characterization of early stages of the damage processes, as nucleation, growth and coalescence of micro-voids and the evolution of the spatial dislocation distribution (dislocation patterning) is a particularly challenging aspect. It was the objective of the work performed to investigate the damage structure near a crack tip by means of small angle X-ray scattering (SAXS).

Pre-cracked fracture mechanics standard specimens from different aluminium alloys and steels were loaded up to different amounts of crack growth. From the crack tip range samples of 100 to 200 µm thickness were prepared and a small region around the crack tip was scanned using a microfocused Synchrotron beam. The SAXS experiments were performed at different Synchrotron sources and equipments with different beam cross section, scan step width and X-ray energy. Additionally, the investigation was completed by other methods like X-ray diffraction, X-ray imaging diffraction technique (MAXIM), transmission electron microscopy, scanning electron microscopy, and positron annihilation spectroscopy.

The SAXS intensity pattern shows location-related effects. Potential SAXS parameters to characterize the damage are the integral intensity, a fractal dimension parameter and a value determined from the ratio of the intensity vertical and horizontal to the direction of crack growth. Above all, the last parameter is suitable to depict the damage zone around the crack tip. It is robust and applicable even for a material which exhibits an anisotropic SAXS pattern in the initial state. The source of this feature is, however, not yet fully understood.

Size and shape of the damage zone determined by SAXS are consistent with the results of finite element modelling.

The result provides a new point of view for evaluating the damage processes in the course of crack initiation and progress.

Contents

Acknowledgements

The author thankfully acknowledges the Marie Curie Fellowships Association of the European Union, within the Improving Human research Potential of the 5th Framework Program, for funding the research.
I am also very much indepted to Dr.Frank Bergner from the Institute of Material Science of the TU-Dresden for introducing me into the general field and for providing the basis of the research, the Al-sheet material sacrificing his sparse material.
I am very grateful to Dr.Wolfgang Tirschler and G.Siemroth at the Institut für Strukturphysik of the TU- Dresden for carrying out the backscatter SEM measurements on our samples and to Dr.Ellen Thiele for carrying out the diffraction experiments and providing the interpretation of the results.
I am very grateful too, to professor Ulrike Schmidt at the University of Halle-Wittenberg who provided the very instructive SEM images and carried out the resistive measurements on the aluminium samples.
I am grateful also to professor Maier, Christiane Zamponi, Stefan Sonneberger and Torsten Staab from the Institut für Strahlen- und Kernphysik, University of Bonn for carrying out preliminary measurements on an aluminium sample using their fascinating Positron Annihilation Microprobe.
I am in deep appreciation of the assistance and quality provided by the beamline responsibles and staff at the ESRF, DUBBLE, Igor Dolbnya and Wim Bras, and ID13, Christian Riekel, Stephan Roth, Manfred Burghammer, HASYLAB, G3, Thomas Wroblewski, Bernd Hasse and BW4, Rainer Gehrke, Sabine Cunis, Willi Fenzl and ELETTRA, SAXS, Sigrid Bernstorff, Michael Rappolt, Heinz Amenitsch.
I am especially grateful to the DUBBLE beamline staff, for introducing the scanning set up, and to the SAXS beamline staff for providing the small beamsize.

From the deepest of my heart, I express my gratitude to everyone at the FZ-Rossendorf who helped me, and I thank them for teaching me how much easier and more efficient it is to work together at all times and immediately help someone with a problem. I thank my institute, the institute for safety research for welcoming me among their midst, I thank professor Frank-Peter Weiss for providing the necessary guidance, I thank the researchers at the Institute of Ion Beam Physics and Material Research, Dr.Norbert Schell (ROBL-ESRF), Dr. Frank Eichhorn, Dr. Friedrich Prokert and Andrea Scholz for providing me with the basic knowledge about X-Ray Diffraction and Scattering and for their assistance and carrying out diffraction measurements, Dr.Arndt Mücklich for carrying out the TEM experiments and helping with the interpretation and Elfi Christalle for carrying out the SEM experiments.
I am very grateful also to Falk Pönisch for helping me out with the programming in IDL.
I am grateful to all collegues at the Department of Material Behaviour and Component Safety, to my chef and supervisor Dr.Jürgen Böhmert, who is an example to me and will stay so, I am grateful for his scientific accuracy always pointing me into the right direction, I am grateful for his leadership, and admire his skill to find a solution to any kind of problem or difficulty and bring out the best in all of us. To our secretary Mrs.Sonja Rott I am grateful for the support she gave, for arranging all administrative matters and for being a good and wise person always ready for a laugh and simply fun to talk to. I am very grateful to all at the workshop led by Ully Skorupa, Jens Pietzsch, Klaus Forker and Bernd Leuner for fitting in the work even when there was no time with such accuracy and efficiency one can only dream of. I am grateful to Michaela Roßner for accurately and finely preparing the samples and always helping out at short notice and simply for being a good collegue. I am grateful to Ruth Opitz for carrying out the metallographic work at the beginning of the fellowship and teaching me

the basics in metallography. I thank Sieglinde Behrens for her very reliable support and poster preparation. I am very grateful to Wolfgang Webersinke for tirelessly repeating to me that we were carrying out the static tension test in the displacement control mode, for his irreplaceable assistance with the tension and three-point-bend testing and for his enthousiasm and linguistic wit. I am very grateful to Dr.Gudrun Müller for offering her time to help me during the many beamtimes at HASYLAB, ELETTRA and the ESRF, for her ability to see changes in the microstructure where no one else can see them and for being a very good friend. I admire Rainer Weiss for providing assistance and support when it was most needed, but also without you knowing making everything work and for his ability to put a smile on my face.
I am thankful to Andreas Ulbricht for always being capable of relaxing a difficult situation with a laugh and for his help with the interpretation of the SAXS-data. I am grateful to Jan Džugan for his help with the fracture mechanics equipment and basic theory and simply for being a good collegue with whom you could share a moment of joy or rain. I wish to thank Detlef Leonhardt for his guidance, for covering for me when a mistake was made and for his company at lunchtime and tea. To Hanno Willschütz I am very grateful for helping out with the little problems that occur now and then and for taking me up in his circle of friends. I wish to thank Dr.Eberhard Altstadt and Dr.Matthias Werner for their valuable help with the Finite Element calculatations and programming. Last, but definitely not least, I am grateful to Dr.Hans-Werner Viehrig for topping up my contract and trusting in my abilities to help with the editing of a conference volume, I thank him for being a good friend and collegue, who with his open and easy sense of humor could turn every situation positive.

I thank all for the beautiful time here full of learning.

1. Introduction

1.1 OBJECTIVES

To establish a method to investigate the large defect gradients near the crack tip and characterize the damage zone by means of Small Angle X-ray Scattering (SAXS).

To investigate the nanosized defects which are expected in the early stages of damage.

The way to achieve these objectives is briefly outlined in the several steps below.
On the basis of earlier studies [GRO,*,**], it became clear that the material had to be sufficiently but not overly ductile to allow ductile crack growth. Furthermore, it was necessary to choose a material which could be prepared relatively easily, could be investigated using synchrotron radiation without extensive background interference and which was commercially attractive. This is described in section 2. Thirdly, the optimal synchrotron source and beamline parameters had to be sought. These are described in section 4.1. Section 4.2 describes how the crack tip can be determined with sufficient accuracy depending on the available beamline components/parameters.
Fourthly, programmes (IDL, Matlab, Fit2D macro) had to be written to read in and process the large amounts of data that arise from scanning applications using 2d-detectors, the main ones are listed in addendum C. Fifthly, from the corrected data, a parameter had to be distilled capable of describing the damage zone around the crack tip in the metals under investigation. This is described and discussed in section 5.

1.2 BACKGROUND

Structural materials, such as bainitic and austenitic steels and aluminum alloys, as used in the nuclear and aircraft, or construction industry, are subject to external stresses in different environments: water, air...
Adopting a damage tolerant design principle, understanding the growth of an assumed preexisting crack under these conditions is of prime importance to prevent extensive crack propagation and failure of the component. Despite the large amount of experimental data and the considerable effort undertaken worldwide, many questions about fracture remain standing. In general, the physics underlying the rate of crack formation and propagation is very complicated. It is, however, well acknowledged that cracks always nucleate at inhomogeneities in the material (grain boundaries, surface heterogeneities, pre-existing microcracks, dislocation tangles). These heterogeneities evolve in time (fatigue, hardening, and void formation). This implies the necessity of a local determination of the plastic (damage) zone and the study of the large defect gradients and defects involved, their size, shape and volume fraction across the region around the crack tip ideally during in-situ deformation.
Scanning and transmission electron microscopy studies of the material require a rather invasive and complicated specimen preparation and provide only two-dimensional information on either 100nm to micrometer-sized structural defects over a large area (SEM) or smaller defects, but only over a tiny volume of material (TEM). Positron Annihilation Microprobe (PAM) seems promising, but provides information over a thin layer of the specimen, so mainly 2-dimensional, nor do the results unambiguously reveal whether the positron trapping centres are dislocation, pores or precipitates.
Thus, in order to investigate the damage mechanisms and the evolution of the damage, it is imperative to obtain information about volume integrative parameters and their evolution and this requires high brilliance experiments at third generation synchrotrons.

Results from previous SAXS measurements [GRO*,**], have shown that: at HASYLAB (JUSIFA), the necked region of Al-samples deformed in tension, showed far greater scattering than the undeformed region and a stretched shape of the scatterers was deduced; these results led to investigations at the ESRF (ID13-MICROFOCUS) using the scanning microbeam (15μmx150μm) which revealed anisotropic scattering attributed to grain boundaries and from which parameters, the integral intensity and fractal dimension were derived and found to describe the damage zone near the crack tip in a bent Charpy specimen. For a coarse grained region, strong anisotropic scattering in the form of streaks were observed and attributed to grain boundary scattering. Preliminary measurements were then carried out at same beamline using a 5 μm x 5 μm beam, but no damage zone was observed. The scan was small and the step width very wide. Furthermore no information was available on the transmission of the sample for each scan point.

1.3 INTRODUCTION TO SAXS

Small Angle X-ray Scattering is a technique which provides structural information on features sized about 1-1000nm. Any scattering process is characterized by a reciprocity law; an inverse relationship exists between particle size and scattering angle. Since the X-ray wavelengths lie around 0.1nm or 1Å, which is much smaller than the features under observation, the corresponding angular range is small, ~0-5°.

X-rays are primarily scattered by electrons. The electrons resonate with the frequency of the X-rays as they pass the atoms of a material and emit coherent secondary waves which interfere with each other. At larger angles the interference is destructive, while at the very small angles, the waves add constructively. Small angle scattering is observed only when inhomogeneities in the electron density of 1 to a few 100nm in size exist.

The scattering curve I, which is obtained from SAXS-experiments can be understood from equation (1.1), which defines the scattering curve as the Fourier transform of the electron distance distribution function p(r).

$$I(q) = 4\pi \int_0^\infty p(r) \frac{\sin qr}{qr} \cdot dr \qquad (1.1)$$

where $q = \frac{4\pi}{\lambda} \sin\theta$ (nm^{-1}) is the value of the scattering vector $q = \left|\vec{k}_0 - \vec{k}_1\right|$, λ (nm) is the wavelength and 2θ the scattering angle.

Before, inhomogeneities in the electron density were mentioned. For dissolved particles, the difference in the electron density of the solute and that of the solvent characterizes the scattering. The scattering amplitude is proportional to this difference, while the intensity is proportional to the square of the difference. The electron density difference is usually termed the contrast, which will be used in the remainder of the text.

The object of the small angle scattering experiments is to determine the size, shape, mass and electron density distribution from the scattering curve I(q) or 2d-image. This, especially for complex systems, can become very difficult and may require advanced models of the system, which in general are not available. A wide range of particle shapes have been modelled and for complex shapes a large number of small, closely packed spheres may be used with which the shape can be approximated. This may be of use for the future, for the development of a model to analyse the scattering curves of complex commercial materials, as those used in the present study.

For the study of metals, alloys, glasses and ceramics, the concept of particle scattering, including interference effects [KRA] is applicable if one phase occurs finely dispersed and dilute among the rest of the substance, which may be the case, roughly, for nanovoids in metals. For polydisperse materials and particle anisotropy, which also applies to the above

materials, the contribution cannot unequivocally be separated from the scattering curve which is flattened out as a result of these influences. Modelling the curve becomes very complicated. To aid in the analysis of complex systems, however, powerful tools exist in the form of parameters which can be determined directly from the scattering curve. These are outlined below.
The first parameter is known as the radius of gyration. It represents the root mean square of the distance of all electrons from their centre of gravity and therefore is an intuitive measure of the spatial extension of the particle. A typical Guinier plot, lnI(q) vs q^2, yields the radius R_G which is proportional to the slope, $R_G = \sqrt{\frac{3}{5}}R$ for spherical particles, $R_G = \sqrt{0.5}R$ for discs or $R_G = \sqrt{\frac{1}{12}}R$ for needles.
Multiplication of the scattering curve by q yields the cross-section factor for rod-like particles. From the Guinier plot, the radius of gyration of the cross section is obtained.

From the scattering curves we obtained for Al-alloys and steels, it was not possible to determine a radius of gyration, because the linear part of the Guinier plot at small q-values, was too short.

A further parameter which may be obtained directly from the scattering curve is the integral intensity, or the invariant Q_0, equation (1.2).

$$Q_0 = \int_0^\infty I(q) \cdot q^2 \cdot dq \qquad (1.2)$$

For a given concentration, its value does not depend on the degree of dispersion.
In section 5.1, the use of the integral intensity within our project is explained more in detail.

Worth noting at this stage, is that the transmitted intensity increases with particle weight, hence also with its volume. For particles with sufficiently homogeneous electron distributions, the volume can be derived from equation (1.3).

$$V = K\frac{I_0}{Q_0}; K = \frac{\lambda^3 a^2}{4\pi} \qquad (1.3)$$

where I_0 is the primary intensity and a the sample-to-detector distance, also referred to as camera length.

A further parameter, the electron distance distribution function p(r) may be obtained from the inverse Fourier transform of the scattering curve, refer to equation (1.1).

Yet, another parameter is known as the mean square fluctuation of the electron density $\overline{(\Delta\rho)^2}$. Please refer to the literature referenced below for further details. For a 2-phase system with known electron density difference, the volume fractions of the phase can be derived.
Our systems consist of several phases, and this parameter was not yet investigated, though maybe it would be interesting from an analogy point of view, to investigate the volume fraction of pores/voids against the rest of the matrix.

A final parameter may be derived from a fit of the tail-end of the scattering curve, a so called Porod plot, with the first term representing the differential scattering cross-section (see also equation 5.2) which represents the scattered intensity.

$$\frac{d\sigma}{d\Omega}(q \to \infty) \approx c \cdot (\Delta n_f)^2 \cdot 2\pi \cdot \frac{A}{q^4} \qquad (1.4)$$

, where c: concentration, Δn_f: the scattering contrast and $A=4\pi R^2$ the surface of a spherical particle. Thus, the asymptotic scattered intensity is proportional to q^{-4}.
For line dislocations, the asymptotic scattering is proportional to q^{-3}, for thin cylinders, to q^{-1}.

In this way, the rough shape of the scatterer can be obtained. In a similar way, a fractal dimension of the scattering yields information about irregular fractal structures.
The use of this parameter is described in section 5.1.

For further reading, please consult references [KRA] and [HAU].

2. Materials

Two metals, Al-alloys used in the air-craft industry and a heat-resistant low-alloy steel were investigated.

2.1 ALUMINIUM ALLOYS

Two Al-alloys were chosen: Al-2024-T351 (Al-Mg-Cu) from Pechiney without cladding, a well known alloy employed in the aircraft industry and Al-6013-T6 (Al-Mg-Si) from Alcoa also without cladding, a new weldable alloy under investigation for use as fuselage material in line with the advanced and more efficient integral fuselage design. Their characteristics, chemical composition (Table 2.1) and tensile data are listed in the tables below.
The 2024 material is a high strength Al-alloy with excellent fatigue resistance, but low corrosion resistance which is why it is commonly used with cladding. It is readily formed in the annealed condition and may be subsequently heat treated. It is readily machined to a high finish. We chose the unclad material to investigate cracking without the cladding influence.
The 6013 material is a weldable alloy with increased yield strength, reduced fatigue crack growth rate, higher toughness and 3% lower density, but also of reduced tensile strength (Table 2.2, UTS).
The Al-alloys were chosen because of their relatively high yield strengths allowing ductile fracture instead of fracture without plastic deformation or failure due to extensive plastic deformation only and because of their major significance in the aircraft industry. Furthermore, with the aim of establishing a method to investigate the crack tip using synchrotron radiation, it proved easier to study aluminium alloys than steels, because of the large fluorescence disturbance from the Fe-matrix taking place at the typical synchrotron radiation energies. In addition, the Al-alloy samples were easier to prepare, because for a given synchrotron radiation energy, ranging from 8-20 keV, the sample thickness ranged from ~80-1000μm, whereas for steel, the sample thickness would have to be ~4-50μm.

Table 2.1: Chemical composition of the Al-2024-T351 and 6013-T6 alloys (wt%)

Material	Cr	Cu	Fe	Mg	Mn	Si	Ti	Zn
Sheet 2024	0.0075	4.18	0.156	1.49	0.686	0.10	0.0098	0.133
SEN(B) 2024	0.0155	4.14	0.179	1.46	0.443	0.12	0.0145	0.190
CT 2024	0.003	4.11	0.05	1.12	0.46	0.048	-	-
Sheet 6013	0.07	0.80	0.09	1.04	0.39	0.65	0.018	0.06

Al: balance

Table 2.2: Tension test data of the Al-2024-T351 and 6013-T6 sheet alloys

Material	$\sigma_{0.2}$ ($R_{p0.2}$) (MPa)	UTS (MPa)	A_g (%)	Fracture strain (%)
2024 L	378	494	14.3	17.4
T	328	486	15.3	17.9
6013 L	370	392	7.3	10.3
T	344	385	7.8	8.2

L,T: Longitudinal,Transverse: loading along or transverse to the rolling direction

The designations -T351 and -T6 stand for specific tempers, T: heat treated to produce stable tempers. -T351 is solution heat treated, stress-relieved stretched and then cold worked to improve strength with a noticable effect in mechanical property limits. T6 is solution heat treated, then artificially aged, not cold worked, without any significant effects in the mechanical property limits. -T6 usually means held at 190° and then quenched in hot water (80°) to arrest/retain the strengthened structure which has formed during ageing.

2.2 STEEL

The 10 CrMo 9 10 steel was chosen, because it was used as a reference material within a research programme [RIC] investigating ductile steels used in the nuclear industry for the construction of the reactor pressure vessel (RPV) and thus represented a well-characterized ductile steel. The steel was designated WS 5E where WS 5 stands for the material type and heat (the chemical composition is given in Table 2.3 below); E characterizes the heat treatment and resulting toughness values for the material (Table 2.4). The material was found to be granular and lath-shaped bainite, ferrite and mixed-carbide, with an average grain size of roughly 20μm [RIC].

Table 2.3: Chemical composition of the WS 5, 10 CrMo 9 10 steel (wt%)

Material	C	Si	Mn	P	S	Mo	Cr	Ni	Cu
WS 5	0.10	0.32	0.55	0.010	0.019	0.96	2.32	0.10	0.15

Fe: balance

Table 2.4: Charpy-V impact and tension test data of the WS 5, 10 CrMo 9 10 steel

Material	nr. of specimens	$\sigma_{0.2}$ MPa	UTS MPa	A_g %	A_5 %	Z %	USE J	T_{68J} °C	R_{ed} MPa	R_{md} MPa
WS 5E	24	630	723	8	21	76	206	-99	776	973

The material was heat treated: austenized at 950°C for 1 hour and quenched in oil;
E stands for the ensuing tempering treatment: held for 2 hours in air at 640°C.

3. Sample preparation

From the original sheet material, M(T)-type (Middle Tension) sheet specimens were spark eroded and notched according to ASTM (American Standard of Testing and Materials) recommendations, vol.03.01, E561 and E-647 [ASTM]. One CT-specimen was precracked and deformed in tension by the GKSS-Geesthacht. The SEN(B)(Single-Edge-Notched-Bend)-specimens were spark-eroded into Charpy-sized (55mmx10mmx10mm) swallow-tailed, notched and side-grooved specimens. More precisely, the specimen had a starter notch of 0.5mm plus a swallow-tail of 2.5mm (90° to the surface), so a total notch depth of 3 mm, and side-grooves of 1mm in depth, 0.4mm radius and flanks at 60°.

The specimen dimensions are listed in Table 3.1. Figure 3.1 shows the standard M(T), Middle Tension, SEN(B), Single Edge Notched Bend, and CT, Compact Tension, geometries.

Table 3.1: Specimen dimensions (in mm)

Material	Specimen	Length	Unclamped Length	Width	Thickness
2024	4.4	252	136	44	1.6
	11.1	190	78	54	1.6
	CT				10
	SEN(B)	55	Span=40	10	10
6013	3.2/3.3	252	148	44	1.6
	10.7b	200	86	54	1.6

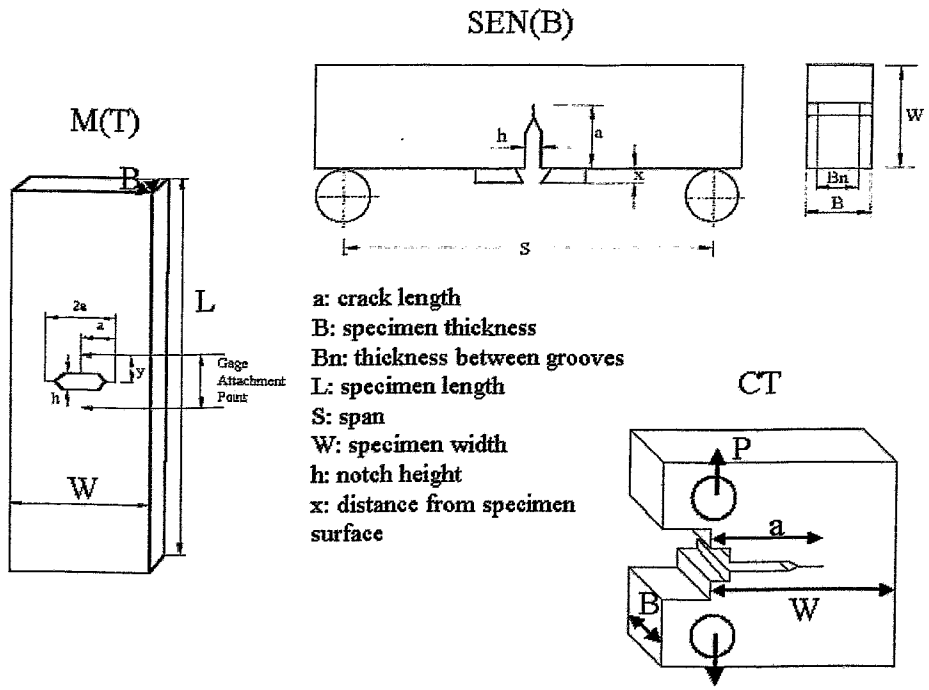

Figure 3.1: The typical geometries: M(T), SEN(B) and CT of the specimens under investigation.

3.1 FRACTURE MECHANICS TESTING

3.1.1 Aluminium

Fracture mechanics tests were carried out mainly to introduce a ductile crack into the material in accordance with ASTM-Standards [ASTM]. For the aluminium sheet and SEN(B) samples one specimen was tested far beyond the force maximum and subsequently broken for later determination of the R-curve for the materials, but the other specimens were all precracked and then deformed in tension or by three-point bending up to force values just below and just above the maximum to introduce a ductile crack and investigate the region prior the extensive crack extension, to investigate the early stages of crack growth. For the M(T) specimens, the crack length data from the crack opening displacement were not very reliable and the region around the force maximum was our best estimate of the blunting region. Figure 3.2 shows the load-displacement diagram obtained from the tests. The crack lengths (optical microscope) for the different specimens are listed in Table 3.2.

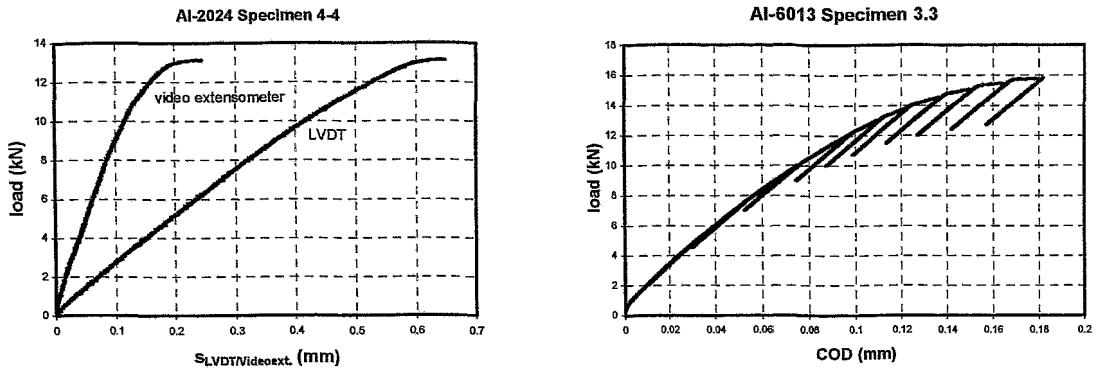

Figure 3.2: Load-displacement diagram for specimens 4.4 and 3.3. LVDT stands for Linear Variable Differential Transformer, COD stands for Crack Opening Displacement which was registered for the 3.3 specimen after mounting on the clamps to hold the COD-gauge, the specimen was deformed using the unloading compliance technique .

Table 3.2a: Crack lengths for the specimens under investigation (in mm)

Material	Specimen	$R_{centre\ hole}$	L_{notch}	$L_{fatigue}$	$L_{crackext}$	$L_{crackvisual}$	$Displ_{max}$
Al-2024-	4.4	0.5	1	11.5	0.24		0.648
T351 (P)	11.1	1.5	4	1.9		2.48	
	CT	-	n.a.	n.a.	n.a.	3.4 (avg)±0.4	n.a.
	SEN(B)	-	2.5+0.5			3.3	
Al-6013-T6	3.3	0.5	1			6.6/6.1(avg)	0.775
(Alcoa)	3.2	0.5	1			4.6	
	10.7b	1.5	4	1.6	0.1	1.8 (avg)	0.24

$R_{centre\ hole}$ is the radius of the hole in the middle of the specimen, L_{notch} is the length of the notch on either side of the centre hole, $L_{fatigue}$ is the length of the crack after fatigue testing, $L_{crackext}$ represents the crack extension from the end of the fatigue crack as a result of the deformation, $L_{crackvisual}$ is the crack length (fatigue+extension) determined using an optical microscope; $\Delta L_{crackvisual}$=0.02mm; $Displ_{max}$: maximum displacement; n.a.: not available: avg: average of two values

Table 3.2b: Crack lengths for the specimens under investigation

Material	Specimen	$L_{crackvisual}$ (in mm)
Al-6013-T6 (Alcoa)	3.3 260µm	Front (marker): 6.66
		Back: 6.48
	3.3 760µm	Front (marker): 6.09
		Back: 6.12
	10.7b	Front (marker): 1.83
		Back: 1.77
A-2024-T351 (P)	11.1	Front (marker): 2.22+tail:0.26=2.48
		Back: 2.49 (end into tail)

P : Pechiney; tail implies crack extension, not observed for 10.7b; Front and Back imply the front and back side of the specimen

3.1.2 Steel

The specimen was oriented in the L-T orientation, which means that the length (55 mm) of the specimen was along the rolling direction, while crack extension ensued in the transverse direction.

Three specimens were prepared. The SEN(B)-specimens were pre-cracked to a/W≅0.48 (a: total notch-crack depth after fatigue, W: width of the specimen) using the RUMOL equipment

at the Department of Material Behaviour and Component Safety at the Institute of Safety Research and two of them subsequently deformed in three-point-bending (MTS-180) up to a value immediately before (E22) and slightly beyond (E21) the force maximum to introduce a stable ductile crack or the beginning thereof.
The visual crack length measured 1.89mm±0.02mm from the notch. This means that the specimen was tested to a/W≅0.49.

3.2 SAMPLE PREPARATION

3.2.1 Aluminium

From the deformed and cracked specimens a small region around the crack tip was cut out by means of spark erosion (Figure 3.3). The specimen was then thinned and polished to a given thickness dependent on the energy of the synchrotron radiation. Accurate thicknesses were obtained using the ACCUSTOP sample holder (STRUERS). Abrasive paper of grain size 100, 220, 400, 600 and 1200 was used after which the samples were polished with 9 µm diamond paste and subsequently on a 3 µm and then 1 µm diamond suspension.
The thicknesses ranged from 80µm-0.8mm (Table 3.3).

Table 3.3: Final specimen thicknesses around the crack tip (in µm), BW4 and DUBBLE

Specimen	**2024ud**	**4.4**	**11.1**	**CT**	**SEN(B)**
Thickness	148	135	135	245	125 BW4
Specimen	**6013ud**	**3.3**	**3.2**	**10.7b**	
Thickness	150	790>283/785 *	136	95	

*One side of specimen 3.3 was measured at DUBBLE in November 2002, this was then thinned for scanning at 10keV and the 2nd side thinned from 1.6mm to 785µm for scanning at 20keV;
ud: undeformed; BW4: beamline at HASYLAB

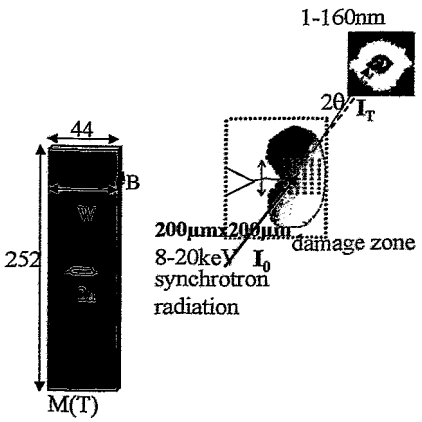

Figure 3.3: From the M(T) (Middle Tension) sheet specimen, a small sample was cut out from around the crack, subsequently thinned and polished to a given thickness (80-800 µm) and placed in the synchrotron beam; B, the specimen thickness, equals 1.6 mm.

3.2.2 Steel

From the deformed and cracked specimen, a smaller sample, E21, of 10mmx10mmx1mm was spark-eroded. This sample was thinned and polished to ~80μm.

3.3 METALLOGRAPHY

For each of the Al-alloys, samples were prepared for grain size determination. For the Al-2024 material, an average grain size of 22-25μm was found. For the Al-6013, the average grain size was found to lie between 46-54μm. Slight variations between the plane of the sample, the surface along the width and along the thickness existed. For the plane of the sample, the surface of the grains was used for the determination, while the grain size was determined from the diameter of the grains for the other surfaces on the sample where a clear preference in the grain direction was found.
Some of the specimens were electrolytically polished to visualize the grains and accurately determine the location of the synchrotron beam with respect to the grain boundaries.
Figure 3.4a shows an undeformed Al-6013 sample, while Figure b shows one of the Al-6013 samples (10.7b) containing a crack at a magnification of ~60x. The photographs were taken three months after the polishing, but the grain contrast is still visible.

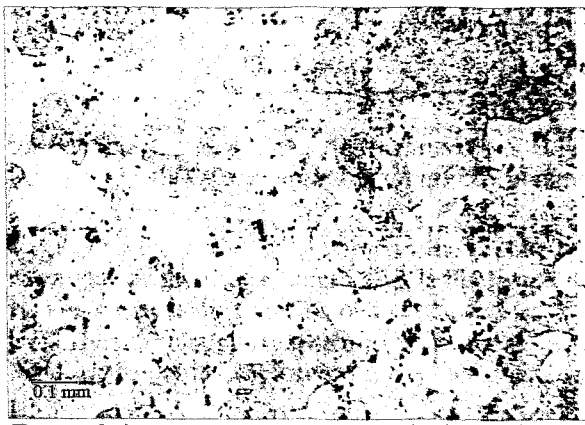

Figure 3.4a: cross-section of the etched undeformed Al-6013 sample.

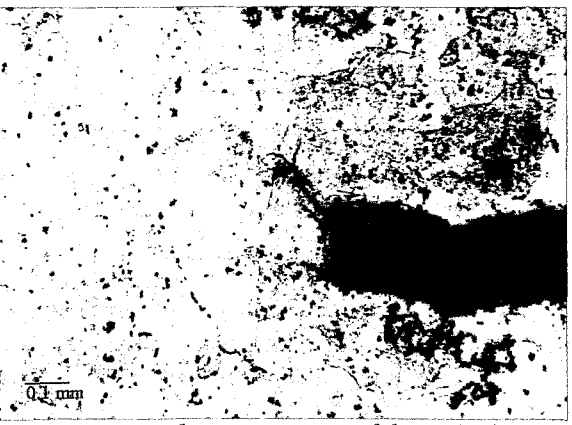

Figure 3.4b: cross-section of the etched Al-6013 sample 10.7b containing a crack.

3.4 FINITE ELEMENT ANALYSIS

To verify the rough shape and size of the damage zone, finite element calculations were performed for samples 4.4 and 3.3.
The result is shown in Figure 3.5a for the Al-2024-T351 alloy and in Figure 3.5b for the Al-6013-T6 alloy.
The damage zone for the Al-2024-T351 specimen 4.4 is sized ~3mm by 6mm (twice the region in the Figure) and ear-lobe shaped.
The finite element data were obtained by networking elements for the M(T)-type specimen (Figure 3.1a) over a quarter (symmetry rules apply) of the specimen. The two-dimensional results were then extruded into a volume, taking into account the thickness of 1.6 mm, but no changes were observed for the overall result.
The results were plotted showing the plastic strain. Later a damage model was implemented, revealing the distribution of the damage parameter, D, [ALT] around the crack tip (Figures 3.5c and d for the Al-2024 and –6013 respectively). The growing crack was simulated using

the opening-node method and by deleting the element for D=1, respectively. The results are comparable.

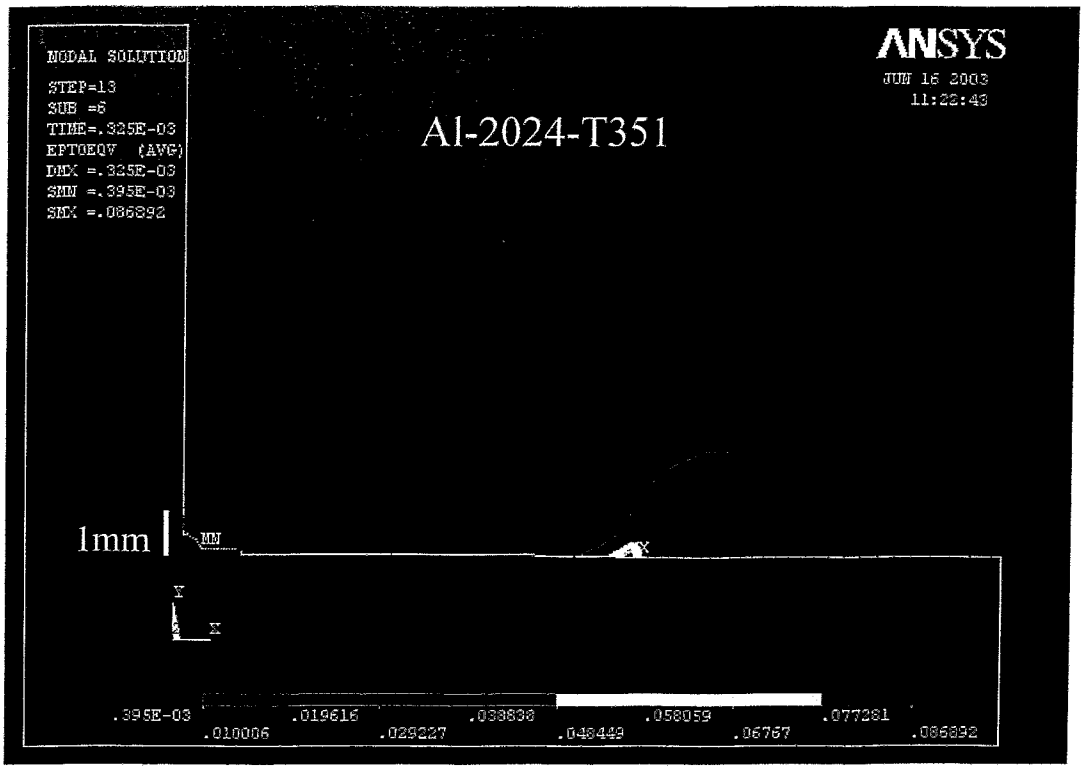

Figure 3.5a: plastic strain from finite element calculations for the 4.4 Al-2024-T351 specimen.

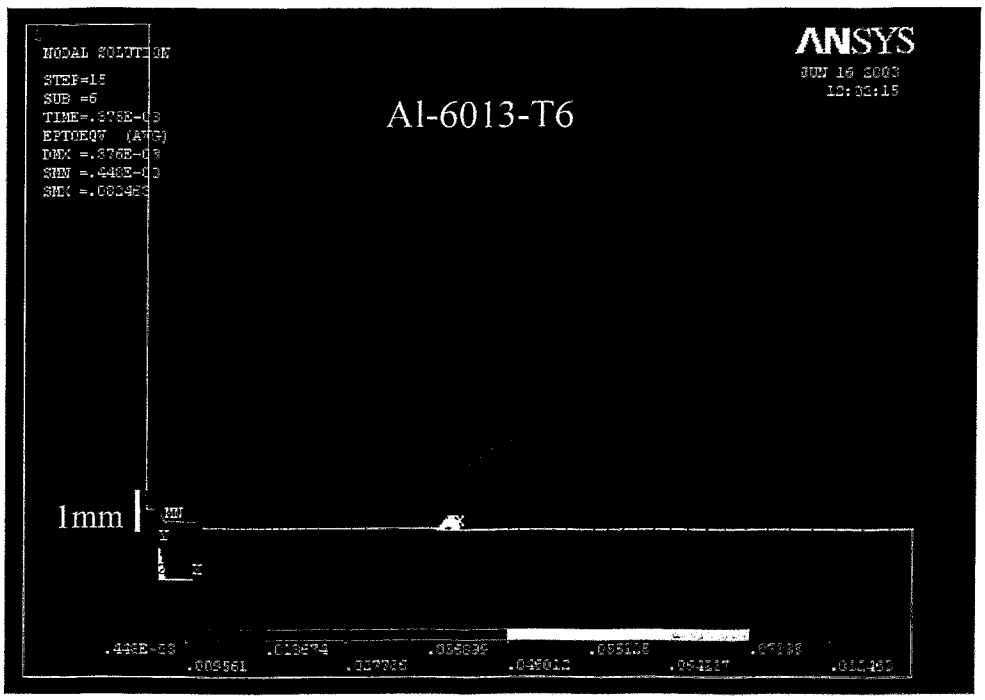

Figure 3.5b: plastic strain from finite element calculations for the 3.3 Al-6013-T6 specimen

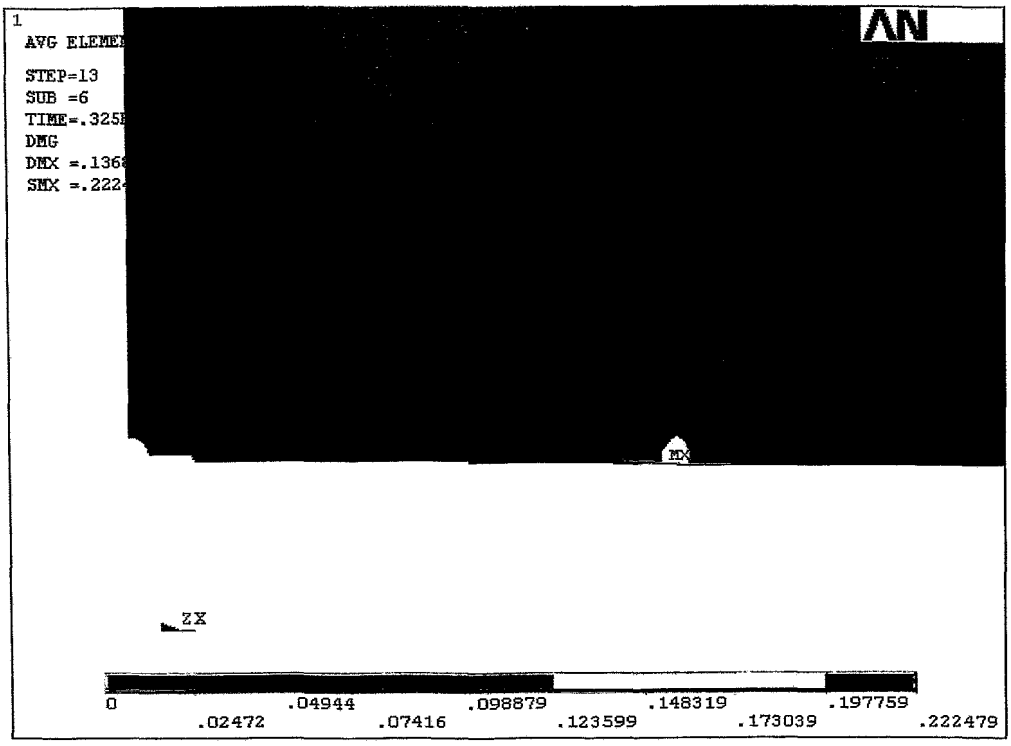

Figure 3.5c: damage D from finite element calculations for the 4.4 Al-2024-T351 specimen.

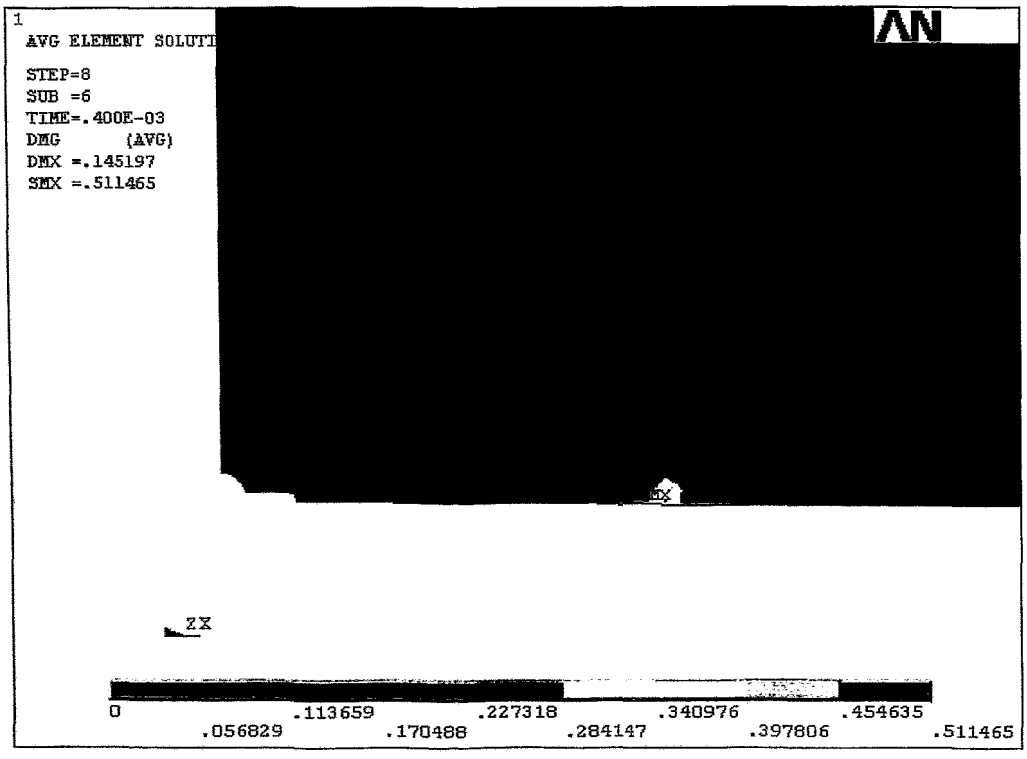

Figure 3.5d: damage D from finite element calculations for the 3.3 Al-6013-T6 specimen

4. Synchrotron sources

4.1 REQUIRED SOURCE AND BEAMLINE PARAMETERS

Our investigations require specific source characteristics and beamline parameters.

4.1.1 Source

Measurements were carried out at three different synchrotron radiation sources: ESRF, HASYLAB and ELETTRA. From these measurements we learnt that for small and very small beam sizes 5-50μm by 5-50μm a collimating system and high brilliance from a third generation synchrotron with undulator devices is required. For small beamsizes up to ~200μm by ~200μm a high brilliance source or medium brilliance source plus wiggler insertion device provides a sufficient intensity. A second important source parameter is the beam stability. Since scanning of a single specimen can take several hours, the stabler the beam, the easier the comparison between the individual scan points.

4.1.2 Beamline

Over the 2-year period measurements were carried out at different beamlines: at the MICROFOCUS (ID13) beamline (ESRF, Grenoble), at the DUBBLE (BM26) beamline (ESRF, Grenoble), at the USAXS (BW4) beamline (HASYLAB, Hamburg), at the MAXIM (G3) diffraction beamline (HASYLAB, Hamburg) and at the SAXS (BL 5.2 L) beamline (ELETTRA, Trieste).

The required beamline parameters are the following:

a. The maximum size of the beam should be around 200μmx200μm, with larger beam sizes a damage zone was also observed, but this is equally feasible with smaller beamsize; the crack tip can be located with more accuracy, and our goal goes to very small beam sizes, for better resolution of the high defect gradients.
b. The beamsize should furthermore either be much smaller or much larger than the grain size of the metal under investigation.
c. The energy has to lie within a range of 8-20keV, higher and lower energies should be possible, but we were limited to this range at the various small angle scattering beamlines. Good results were obtained within this range;
d. There has to be an accurate means to determine the transmitted intensity, preferably also the direct beam intensity for each scan point. The variation of the sample thickness at best lies around 20μm, but has often been more and without correction for the thickness, thus transmission, all information in the total or integral, intensity differences per scan point is lost. This is presumable what happened at ID13, where at that time no intensity detection per scan point was available and the specimen was thicker near one edge.
e. There has to be a means to detect the transmitted intensity or a microscope (optimal) to locate the crack tip; this is implicit when d. is the case, and otherwise usually available in the form of a photodiode which may be placed into the transmitted beam;
f. In the case of very small beam sizes, $\leq$ 50 μm, there has to be a collimating system, for larger beam sizes, a set of slits and guard slits cutting away part of the beam still allows sufficient intensity; a collimator was available only at ID13, Grenoble; at the other beamlines it was ill-advised to go to ~100μm beam sizes, only at ELETTRA it was attempted, but the intensity was very low and the disturbing scattering off the slits meant that the beamstop was larger than optimal.

g. Changing the beamsize has to be an option; this, in principle is an option, but not standard practise and requires a lot of setting-up time; best would be to measure the samples at ~200 μm, change the beamsize once and remeasure the interesting regions of the samples using a smaller beam size (5-10 μm), though sample mounting can also be time consuming, e.g. when the crack has to be located.
h. The beamstop size has to be optimal, cover the transmitted beam only; this is not evident for smaller non-standard beamsizes and variable sample-to-detector distances;
i. The distance between specimen and detector should be large enough to investigate at high energies, e.g. 20keV for steel specimens, which would have to be too thin at lower energies and still investigate the scattering which is most pronounced in the lower q-range, see table 4.1;
j. There should be a scanning programme available which connects the motor control with the data acquisition; a full two-dimensional scanning set up was available at first only at ID-13, partially at BW4 and ELETTRA and asked for and obtained in full at DUBBLE. A scanning set up allows more efficient, ordered and far less tedious data collection.

Remark to point g.
As an example, considering a measurement time of 30s per scan point, a scan region of 4mm by 2mm and a beam size of 10μm. Scanning the entire region at a step width of 10μm, would imply around 14 days of measurement time per specimen. Since hardly ever more than 3 days are attributed at these highly desired beamlines, such a demand is not possible, and a change of the beamsize is needed.

Unfortunately, none of the beamlines offered perfect conditions, though improvements were made as a result of our requirements.

Table 4.1 lists the most important measurement parameters for each beamline.

Table 4.1: Comparison of the beamline parameters

Beamline/parameter	MICROFOCUS	DUBBLE	USAXS	SAXS
Brilliance [5]*	highest (und)	high (bm)	high (wig)	high (wig)
Energy (keV) *	12.7	20, 12.38, 10	10.1	8
Beam size at sample (mm)*	0.005 by 0.005	0.2 by 0.2	0.4 by 2	0.07x0.2
Intensity measurement [4]*	n.a. [3]*	2	3	1+1
Camera length (mm) [2]*	498	8100	12469	2510
Q-range (nm^{-1}) *	0.08-1.04	0.04-0.58 $_{10keV}$ 0.08-1.17 $_{20keV}$		0.06-0.93

und:undulator, bm: bending magnet, wig: Wiggler; *values correspond to those chosen for the experiment; [2]*sample-to-detector distance; [3]* an ionization chamber has recently been installed; [4]* 2: two ion chambers; 3: two ion chambers plus photodiode at detector; 1+1: one ion chamber plus one mobile photodiode; [5]* [BAL] Where the brilliance represents a physical quantity of the X-ray source which allows comparison between the sources.

$$brilliance = \frac{photons / \sec}{(mrad)^2 (sourcearea, mm^2)(0.1\% bandwidth)}$$

where $mrad^2$ describes the beam divergence, and 0.1% bandwidth is a measure of the photon energy range which is independent of the actual energy.

4.2 LOCATION OF THE CRACK TIP

Different beamlines imply different experimental setups. The techniques and hardware components used to detect the transmitted beam and the method used to detect the crack tip and the width of the crack at the tip to an accuracy of ~10 μm is described below.

At the MICROFOCUS beamline a very precise and reliable system is used.
The scanning setup is equipped with a high-resolution microscope located at a calibrated distance from the beam position. A specific point can be selected on the sample and automatically transferred into the beam. This is simple for thin samples which are lit using the microscope in transmission. For thicker samples, such as ours, the reflected beam has to be used, this requires some adjusting.
A frame grabber image (Figure 4.1) is shown below.

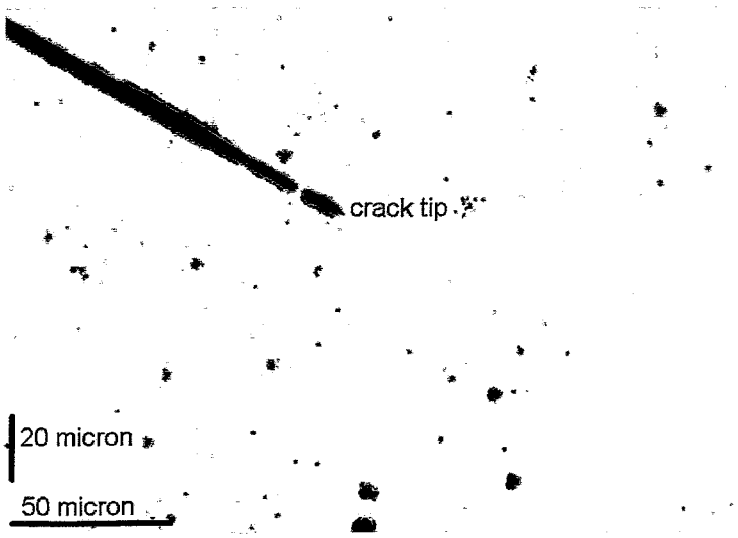

Figure 4.1: Optical microscope view of the crack and crack tip.

At the DUBBLE beamline the advantage is that two ionization chambers are available, one in front of and one behind the sample stage, which provides the intensity at every scan point. In this case, the crack tip can be determined scanning across the sample. Best is to mount the specimen such that the crack is either vertical or horizontal, this can be checked by scanning across the edges and recording the ionchamber 1 and 2 data. The accuracy is improved with smaller beam size and step width, a step width smaller than the beam size is not superfluous and improves the resolution.
At the USAXS beamline two ionization chambers are also available plus a photodiode at the position of the beamstop. This also provides a means to determine the direct beam as well as the transmitted intensity for each scan point and allowed us to scan the specimens to locate the crack. This configuration allows the determination of the purely scattered intensity by subtracting the intensity at the beamstop from that in ionization chamber 2 containing scattered and transmitted intensities. At BW4, it is furthermore possible to register the positron current in the (DORIS, HASYLAB) ring which may vary and cause stray peaks which may then be filtered out, also by using ionchamber 1, and are not mistaken for e.g. the crack.
Figure 4.2 below shows a horizontal scan across the sample holder containing all seven specimens and a specimen for calibration, from left to right: a calibration specimen (calib.), undeformed 2024-T351, undeformed 6013-T6, deformed 4.4 2024-T351, deformed 3.2 6013-T6, deformed 11.1 2024-T351, deformed 10.7b 6013-T6, deformed SEN(B) 2024-T351. The

small peaks in the centre of each scan across a specimen reveal the cracks in the specimen; the undeformed samples of course have no cracks. The peaks off the sides relate to the edges of the holes of the sample holder.
A remark on the specimen holder is useful at this stage. The BW4 specimen holder was optimal and used also at ELETTRA, because the holes were large enough to fit the whole specimen showing also the wider portion of the crack simplifying the location of the crack and showing the uncracked ligament.

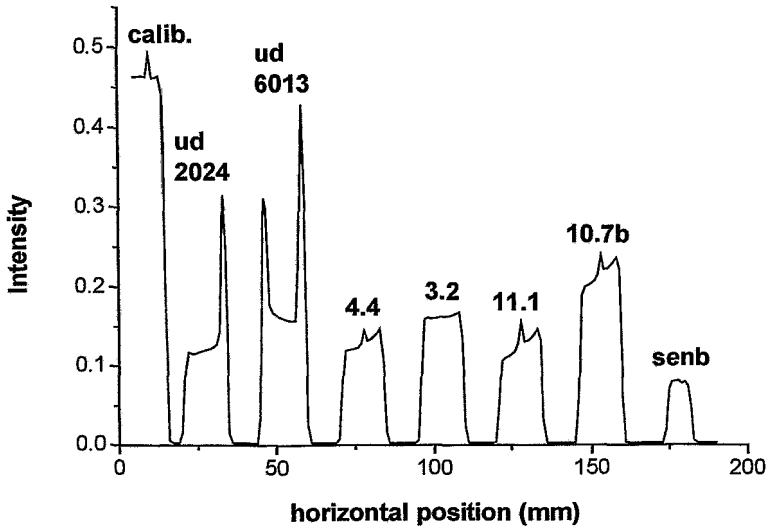

Figure 4.2: Horizontal scan (ionization chamber 1) of the sample holder, with central peaks corresponding to the cracks and border peaks corresponding to the edges of the holes of the sample holder.

The small centre peaks were then scanned with a finer scan step: 50μm (Figure 4.3) compared with 1mm for the large scan (Figure 4.2), and in this way, by repeating such small step horizontal scans at increasingly lower vertical positions, the crack tip was found for each deformed and cracked specimen.

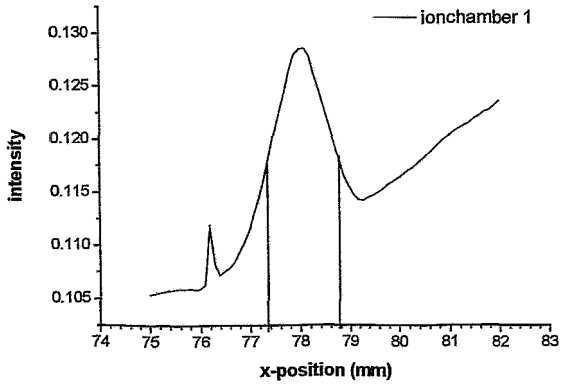

Figure 4.3: Horizontal scan (ionization chamber 1) of specimen 4.4, revealing the crack at a horizontal position near the tip (78,11).

At the SAXS-beamline in Trieste, the small beamsize: ~50μm by 200μm allowed us to refine this technique using increasingly smaller stepwidths to locate the crack tip using ionization chamber and photodiode.
To summarize, finding the location of the crack tip is optimal using a calibrated microscopic image, but this is rarely available. The crack tip may be determined to a sufficient accuracy using a photodiode or ion chamber, located behind the specimen, between specimen and detector, while scanning with a finer beam and eventually with small step width. Preferably, this is carried out while registering the direct beam which may fluctuate.
Some doubt may arise as to where the crack tip is actually located, e.g. when metallographic images show different crack lengths for the two faces of the specimen or show the crack and where it ends, but with a very narrow crack extending beyond the obvious end (Figure 3.3b). The difference between the crack end can amount to 1 mm (CT-sample). Once the true end is chosen, the accuracy of the crack tip location can be calculated.
For our measurements, it was determined to be 2 μm when using a microscopic image.
For a crack tip width of ~100 μm, when using the transmitted synchrotron radiation with fine beam and step width, e.g. 200μm and 50μm respectively, the accuracy amounts to 30 μm.

5. Results and Discussion

This section will describe three damage parameters which were investigated as potential parameters to characterize the damaged region around the crack tip and discuss further analysis of the scatterer(s) responsible for the pattern.

5.1 DAMAGE PARAMETERS

The three damage parameters are named the **integral intensity** or **invariant Q_0**, the **anisotropy parameter** and the **fractal dimension parameter**.

5.1.1 The integral intensity

The integral intensity is given by equation 5.1.1.1, see also equation 1.2 in section 1.3.

$$Q_0 = \int_0^\infty q^2 dq \cdot I(q) \qquad (5.1)$$

where q is the scattering vector [nm^{-1}] and I represents the scattered intensity.

Q_0 was determined from the azimuthally integrated intensity I(q) by calculating the area $q^2I(q)\bullet\Delta q$ for each scan point of the region scanned around the crack tip, after standard corrections for detector dark current, background and transmission.
The procedure is visualized in Figure 5.1, Δq was varied to eliminate experiment inaccuracies (addendum B).

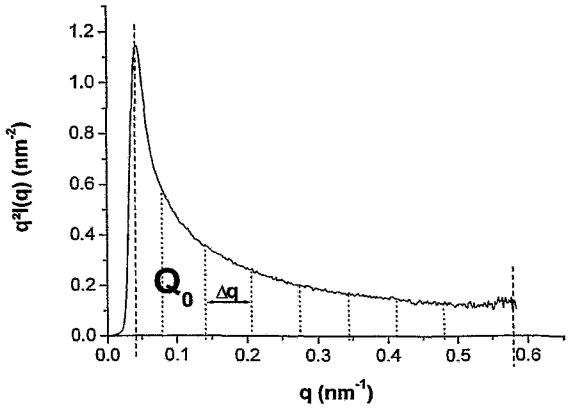

Figure 5.1: Visualization of the procedure to determine the integral intensity Q_0 from the area under the curve.

Q_0 was then plotted for each scan point to visualize this parameter for the entire scan region. Figure 5.2a shows the result for an Al-6013-T6 specimen (3.3) ~283µm thick, measured at DUBBLE, Grenoble at 10keV. There is, however, no clear contour of a damage zone around the crack tip as schematically portrayed in Figure 3.3. An almost horizontally stretched intenser region is seen immediately below the crack tip, which extends towards the crack tip, but it does not depict the expected shape. A scan of the undeformed sample yields lower values, but somewhat too low values, which, however, is likely due to the difference in the specimen thickness. Though corrected for transmission, the amount of scatterer in the thinner sample can differ. It has to be noted here, that the 283µm thick sample is actually too thick for optimal transmission at 10 keV.

Figure 5.3 shows the same sample measured at 20 keV. At this energy, the q-range is slightly shifted to higher values, therefore the range of the size of the scattered defects is shifted towards slightly smaller defects and a large damage region is visible ahead of the crack tip.

Figures 5.4a and b show the integral intensity for a thicker sample from the same M(T)-specimen, taken from around the other crack on the other side of the centre hole and notch. Here two crack tips can be detected, each of them showing a small damage zone immediately ahead of the crack tip, accompanied by a stretched region of high intensity above.

What can be learned at this stage is that the integral intensity is sensitive to a particular type or particular types of scatterers, some of which are already present in the undeformed material. It is unclear how to distinguish between the scatterers caused by the deformation and those already present in the material.

The size range of the scatterers at 10 keV lies roughly around 11-165 nm (q: 0.038-0.583 nm^{-1}) and around 5-70 nm at 20 keV (q: 0.089-1.164 nm^{-1}). Since no increased scattering ahead of the crack tip is seen for the 283µm thick Al-6013 sample at 10 keV, but indeed for the sample at 20 keV, one could assume that the scatterer(s) which cause the increased scattering in Figure 5.3 are between 5 and 11 nm in size, but as will be seen later, this assumption will not hold.

Furthermore, the integral intensity is sensitive to the crack itself. It is thought that using a ~200µm by 200µm beam, the edge(s) of the crack can be illuminated in the scan which of course represent a strong scattering contrast and explains the increased intensity along the crack, but also means that the crack itself can be followed accurately in the image.

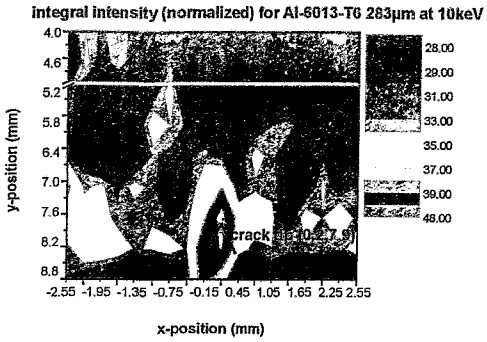

Figure 5.2a: the normalized integral intensity for the deformed Al-6013 alloy at 10keV shows. a stretched zone below the crack tip.

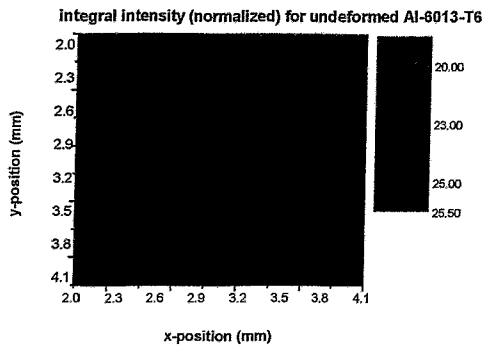

Figure 5.2b: the normalized integral intensity for the undeformed Al-6013 alloy at 10keV shows no pattern and much lower values.

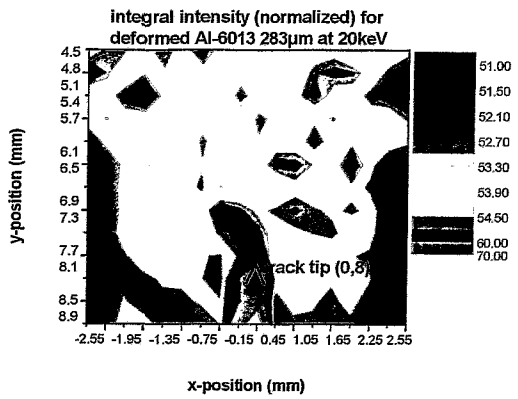

Figure 5.3: the integral intensity for the deformed Al-6013 sample at 20keV reveals a large, but scattered zone ahead of the crack tip.

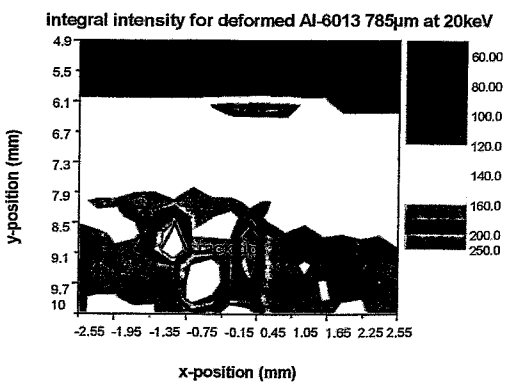

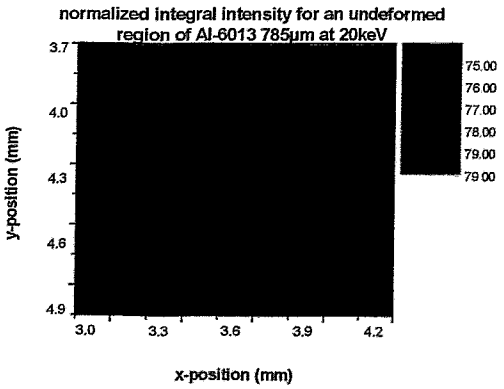

Figure 5.4a: the integral intensity parameter for the deformed Al-6013 785µm specimen at 20keV shows two cracks extending into a small damage zone.

Figure 5.4b: the integral intensity parameter for an undeformed region at 20keV shows no pattern.

Figures 5.5a and b show the integal intensity for the steel sample around the crack tip and for a region away from the crack, respectively. A damage zone ahead of the crack tip is clearly visible and the integral intensity outside of the crack region is clearly lower. The lower edge in Figure a is due to scattering off the edge of the sample/sample holder, while the wide notch leading into a crack for this three-point-bend sample clearly depicts the wider part of the crack in which no scattering takes place by a very low integral intensity.

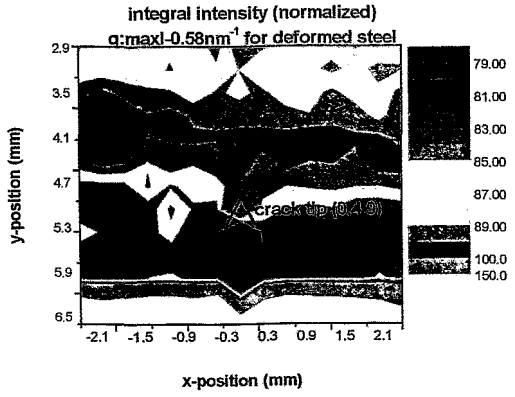

Figure 5.5a: the integral intensity for the deformed steel sample shows a clear stretched damage zone ahead of the crack tip.

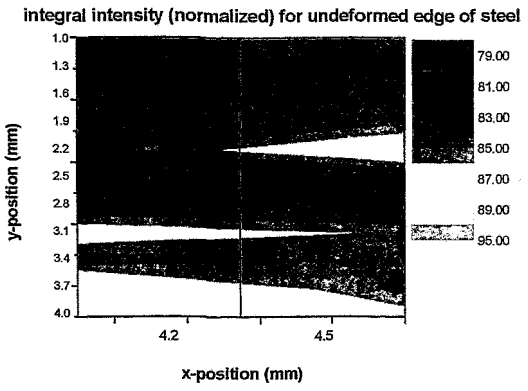

Figure 5.5b: the integral intensity for an undeformed region of the steel sample shows no pattern and lower values.

5.1.2 The total intensity

Because the integral intensity, especially in Figures 5.2 and 5.4, did not show a clear damage zone ahead of the crack tip, an alternative to the above determination was tested.
Instead of the integral intensity, which is an invariant and a well-known parameter in small-angle-scattering experiments, the total intensity on the detector was determined and visualized. Figure 5.6a, shows this intensity parameter for the Al-6013 alloy at 10keV. Figure 5.6b, shows the corresponding results for the undeformed material.

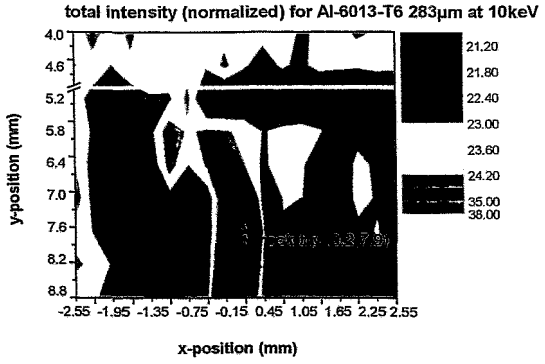

Figure 5.6a: the total intensity for the deformed Al-6013 alloy at 10 keV shows a zone of increased intensity ahead of the crack tip.

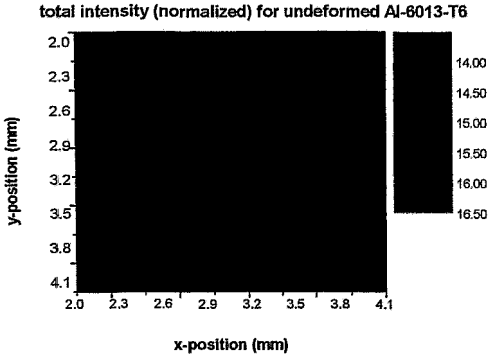

Figure 5.6b: the total intensity for the undeformed Al-6013 alloy at 10 keV shows no pattern and much lower values.

Figure 5.6a shows an increased intensity immediately ahead of the crack tip, but the zone is not clear. At the left and top border of the scanned region, the intensity is high. Again this is related to the interference of scatterers already present in the undeformed material. The values for the undeformed sample are much lower, but the variation in the intensity from orange to green is about 1.5, while the variation for the undeformed material is more than 2. The lower values may be related to less overall scattering from the thinner (150µm) undeformed sample. By comparison, the total intensity does seem to show a damage zone ahead of the crack tip which was not observed in the integral intensity, though some questions remain, and absolute proof that the increase in intensity is significant remains elusive.

Figure 5.7 reveals a result for the total intensity of the same sample measured at 20 keV which is similar to that obtained for the integral intensity and clearly depicts a damage zone ahead of the crack tip.

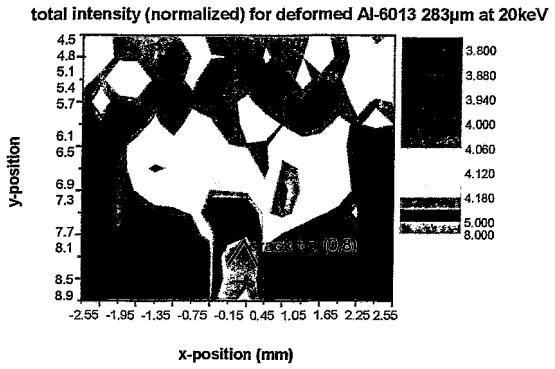

Figure 5.7: the total intensity parameter for the deformed Al-6013 283µm sample at 20keV shows a damage zone ahead of the crack tip.

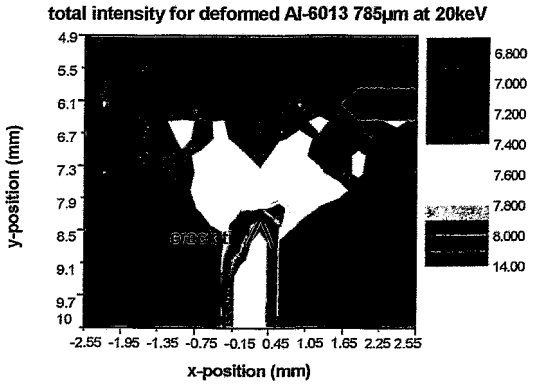

Figure 5.8a: the total intensity for the deformed Al-6013 785µm specimen at 20keV shows a damage Zone ahead of the crack tip in the centre.

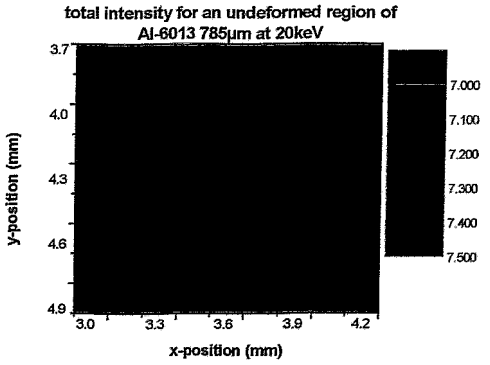

Figure 5.8b: the total intensity for an undeformed region at 20keV shows no pattern an low values.

Figures 5.8a and b show the total intensity for the thick, 785µm, sample measured at 20 keV and indeed (Figure a) reveals a damage region ahead of the centre crack, yet does not show the second crack, observed for the integral intensity, more to the left. The scan of the same sample over a region far outside the crack region (Figure 5.8b) shows values corresponding to the region outside of the crack surrounding the damage zone in Figure 5.8a and shows no pattern. This provides proof that the increased values observed in figure a are meaningful.
For the steel sample, a damage zone is also observed, though, the shape is triangular rather than stretched as observed for the integral intensity. The crack is also perceived in black indicating a very low scattered intensity from the crack which is self evident. For the scan of the undeformed region on the sample, the intensity is lower and no pattern is visible.
The results for the other samples, fatigued Al-6013 and CT, and for the samples measured at BW4, HASYLAB, are presented in addendum A.

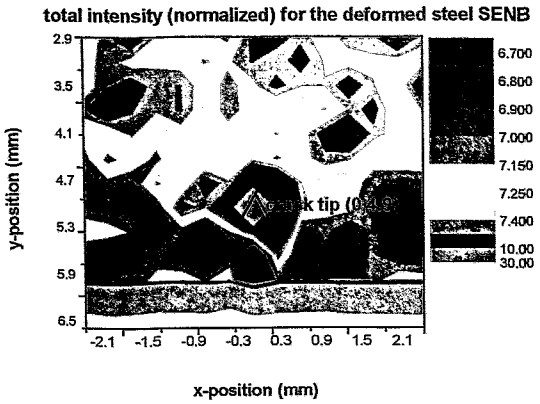

Figure 5.9a: the total intensity parameter for the deformed 10 Cr Mo 9 10 steel shows a large damage zone around the crack tip.

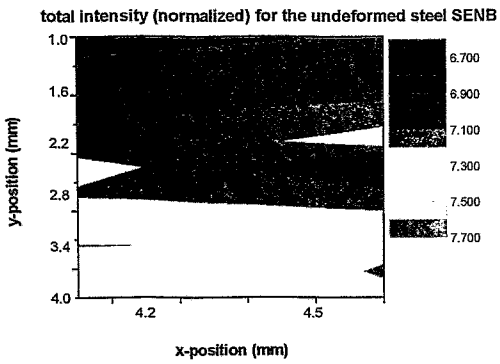

Figure 5.9b: the total intensity parameter for an undeformed region of the steel sample shows no pattern and lower values.

5.1.3 The anisotropy parameter

The anisotropy parameter was determined as depicted in Figures 5.10a-c. From the scatter images plotted for each scan point in the two-dimensional scan in Figure 5.10a, an anisotropy can be seen very clearly for the Al-2024-T351 alloy.

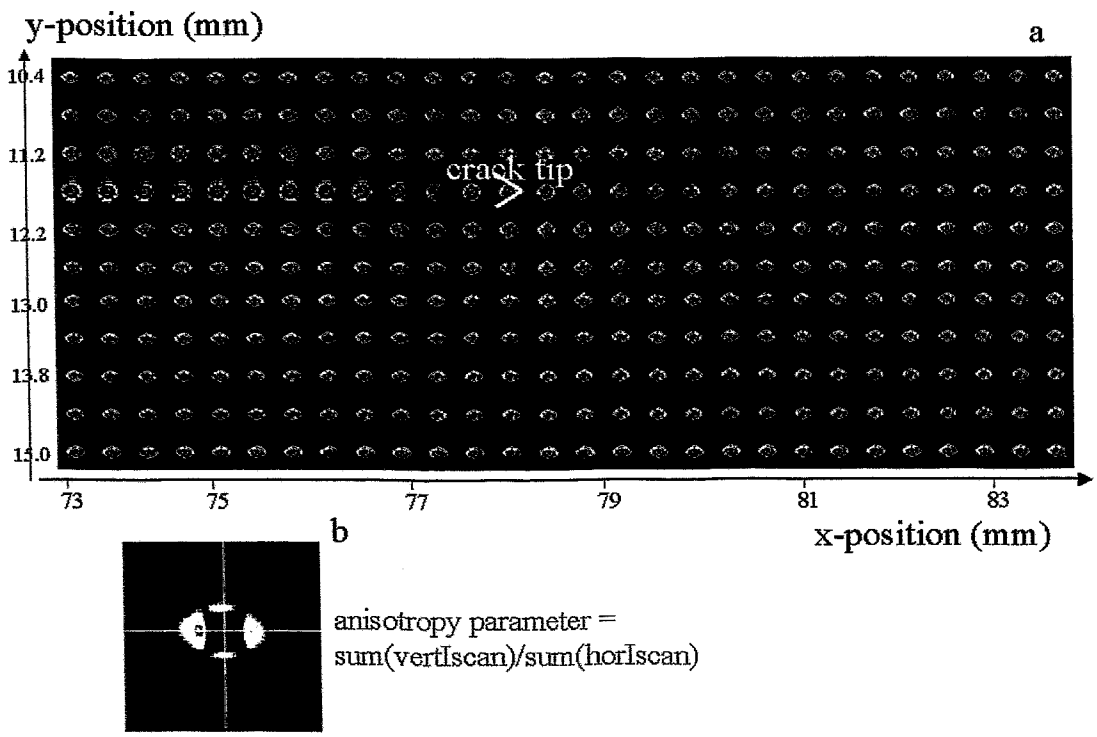

Figure 5.10 a, reveals the scatter images for each scan point across the scanned region including the crack; b, depicts how the anisotropy parameter is determined from a single scatter image.

The crack tip is located at (78.0,11.5)mm ±0.2mm. At the crack itself, the scattering seems isotropic and clearly outlines the crack path. Away from the crack, a strong anisotropy is observed; in the horizontal direction (parallel to the crack), the scattering is stronger than in

the vertical direction. This appears to be related to the rolling direction. Most importantly, this anisotropy is changed around the crack tip; the stretching in the vertical direction, perpendicular to the crack becomes stronger.
This anisotropy was then parametrized by summing all the corrected intensities of the channels in the scatter image for one column going through the beam centre and for one row also through the beam centre (Figure 5.10b) and subsequently dividing these sums, thereby increasing the anisotropic effect.
This anisotropy parameter was then plotted for each scan point as shown in Figure 5.10c which clearly depicts a damage zone around the crack tip where the parameter values are noticeably different from those outside of the crack region. In addition the values are lower and on average vary less for a scan of an undeformed specimen (Figure 5.10d).

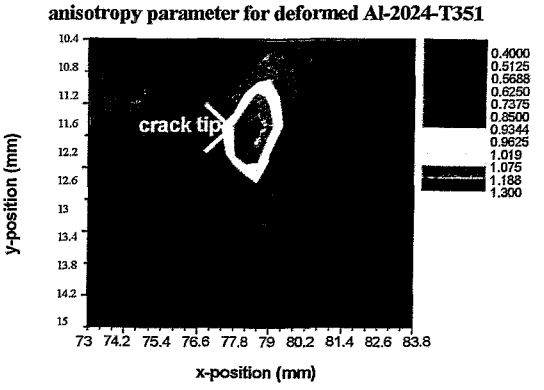

Figure 5.10c: the anisotropy parameter for the deformed 4.4 Al-2024-T351 alloy clearly shows a damage zone around the crack tip.

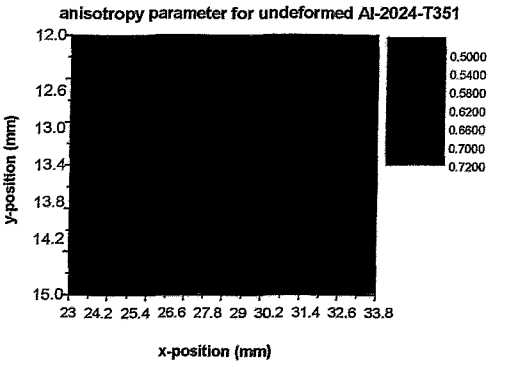

Figure 5.10d: the anisotropy parameter for the undeformed Al-2024-T351 alloy does not reveal any pattern.

On this basis, the anisotropy was investigated further and also found for the Al-6013-T6 alloy, though less pronounced also in the direction parallel to the crack (Fig. 5.11a, specimen 3.3). Around the crack tip, the anisotropy appears stronger in the horizontal direction, which for this sample is transverse to the crack.
The anisotropy parameter clearly reveals a damage zone ahead of the crack tip, but important data from y = 4.3-7.0 mm are missing. Figure 5.12, however also reveals the anisotropy parameter for this specimen at the higher energy of 20keV. Here, the damage zone is clearly visible and appears roughly similar to that at 10 keV; the shape almost represents the standard textbook shape of a damage zone around a ductile crack. The undeformed specimen, Figure 5.11c, shows no pattern and lower values corresponding to the undamaged region, though also somewhat lower than the values surrounding the damage zone in Figure b.
On average, and compared with the integral and total intensity, the damage region obtained plotting the anisotropy parameter is much clearer delineated for all specimens.
Similarities are found for each of the samples, either between integral intensity and anisotropy, a damage zone around the left crack for the 785μm thick Al-6013 sample (Figures 5.4a and 5.13a) or between the total intensity and the anisotropy, as for the 283μm thick sample at 10 keV (Figures 5.6a and 5.11b).
For the 283μm thick sample at 20 keV, closer correspondence in the shape of the damage region is observed for all three parameters.

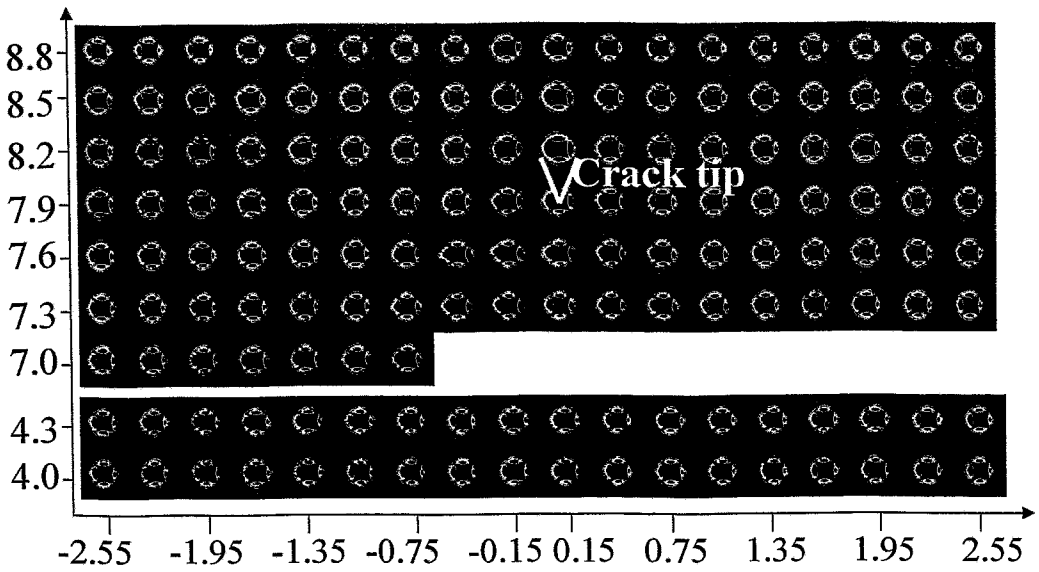

Figure 5.11a: the scatter images for the Al-6013 alloy, specimen 3.3 for each scan point across the scanned region including the crack (viewed upside down).

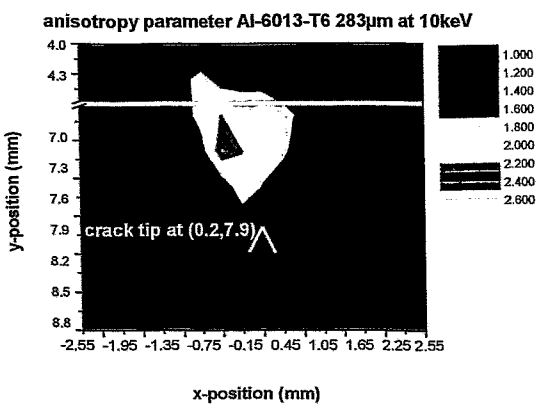

Figure 5.11b: the anisotropy parameter for the deformed Al-6013-T6 alloy clearly shows a damage zone around the crack tip.

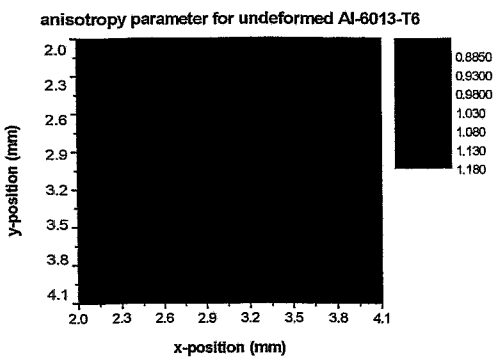

Figure 5.11c: the anisotropy parameter for the undeformed Al-6013-T6 alloy shows no pattern.

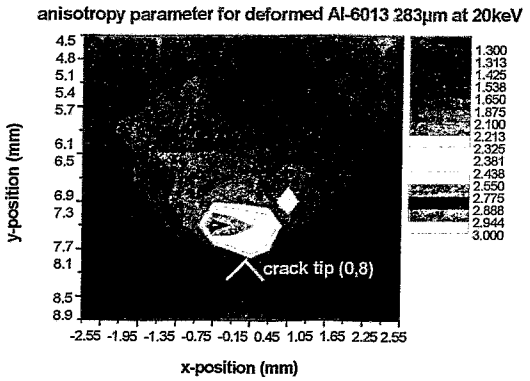

Figure 5.12: the anisotropy parameter for the deformed Al-6013 283µm specimen at 20keV clearly shows a damage zone ahead of the crack tip.

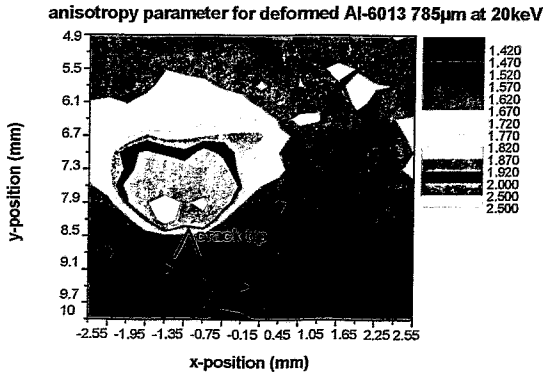

Figure 5.13a: the anisotropy parameter for the deformed Al-6013 785µm specimen at 20keV reveals a damage zone ahead of the crack tip on the left.

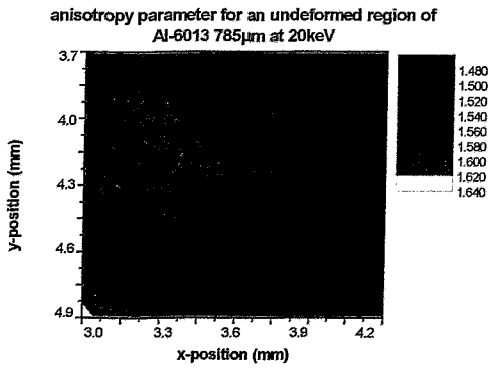

Figure 5.13b: the anisotropy parameter for an undeformed region at 20keV shows no pattern and lower values.

For the steel SEN(B) sample, a form of anisotropy was also observed, Figure 5.14a.
Figure 5.14a already reveals the presence of a damage region ahead of the crack tip in the higher intensities for some of the points. Figure 5.14b shows the anisotropy parameter which clearly visualizes the damage zone around the crack tip, whereas no pattern and lower values are observed from Figure 5.14c representing the undamaged region close to the edge of the sample.
The increased scattering seen in the top row at position y=6.2 mm has to be attributed to scattering off the edge of the sample/sampleholder (Figure 5.14a).

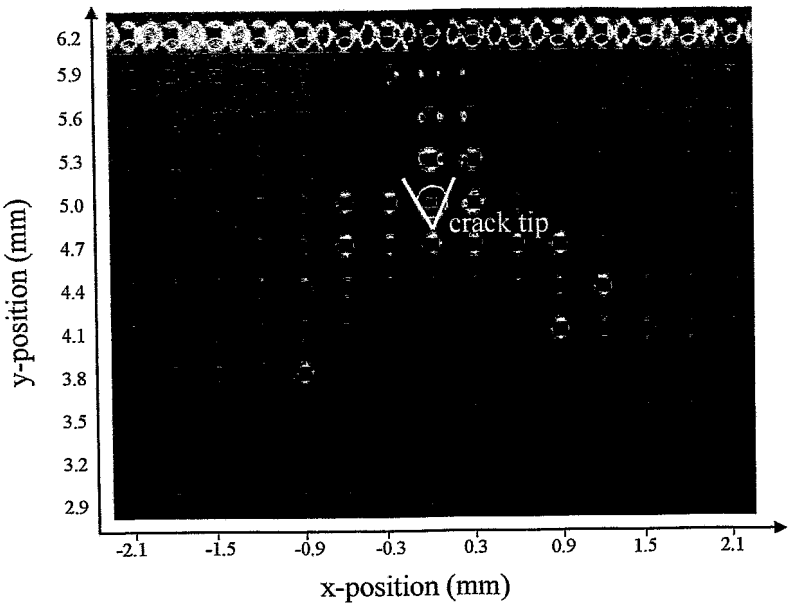

Figure 5.14a: the scatter images for each scan point across the scanned region including the crack at the bottom centre (viewed upside down)

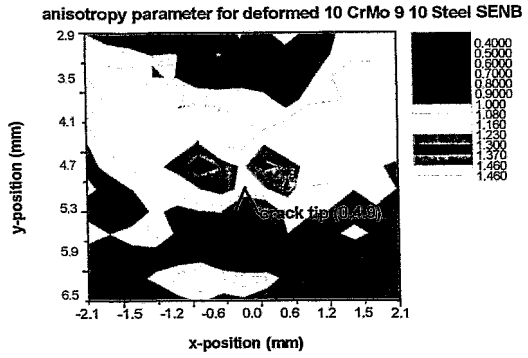

Figure 5.14b: the anisotropy parameter for the deformed 9 Cr Mo 9 10 clearly shows a damage zone around the crack tip.

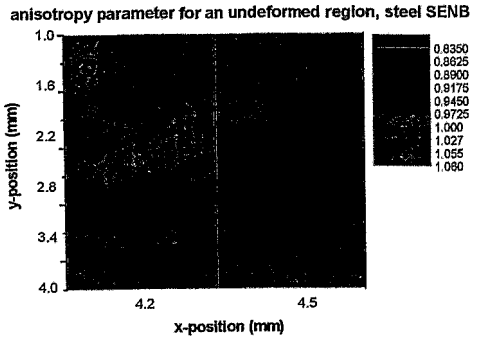

Figure 5.14c: the anisotropy parameter for an undeformed region of the sample shows no pattern and lower values.

At this stage it is important to note that for each parameter and each sample, a clear gradient in the value of the parameter corresponding with the distance from the crack tip can be seen. It would be interesting to focus on a small highly intense region closest to the crack tip and scan it using a fine microbeam to ascertain the defect gradients within this region and investigate possible void structures.

5.1.4 The fractal dimension

The fractal dimension parameter relates to the power of q^{-1} with which the intensity or scattering cross section drops, equation 5.2.

$$\frac{d\sigma}{d\Omega} \propto q^{-n} \qquad (5.2)$$

where the first term represents the differential scattering square cross section ($d\sigma$), the scattered intensity per atom of scattered material expressed in multiples of the scattering intensity from one electron, and $d\Omega$ the spatial angle, n is the fractal dimension.

In some growth processes, strong irregular fractal structures may be formed. A distinction is made between mass or volume (n=1…3) and surface (n=3…4) fractals.
For mass fractals, the mass m of the fractal structure relates to its radius R according to the following equation.

$$m \propto R^n \qquad (5.3)$$

For surface fractals, the size of the rough surface, A, relates to the object size, with radius R, as follows.

$$A \propto R^{n-1} \qquad (5.4)$$

The asymptotic region of the curve of the azimuthally integrated I(q)-data (logarithmic) was fitted according to equation (5.2) (see also section 1.3), see Figure 5.15 and Table 5.1 listing the q-ranges expressed in channels out of 365.
In 'The fractal geometry of nature' by B.Mandelbrot [MAN], the concept of a fractal describes objects which are self similar, objects for which one cannot speak of a characteristic size; the concept of the fractal dimension is explained.

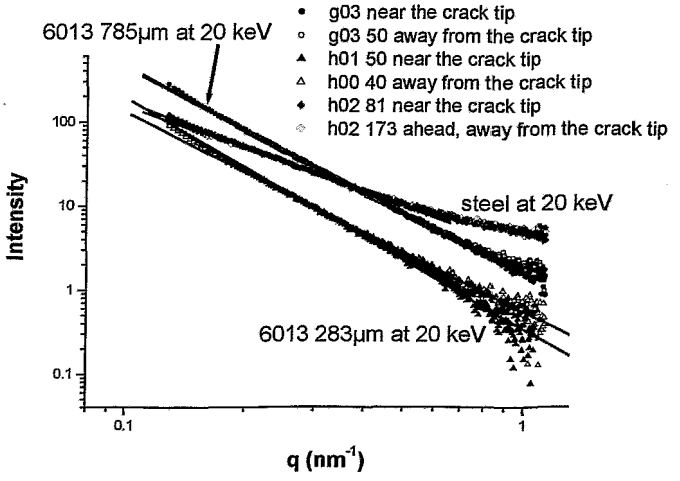

Figure 5.15: For the steel and Al-6013 alloy in the region of the crack tip and farther from the crack tip, the fractal dimension parameter n is determined from a fit of the slope of a log-log plot of the scattering curve I(q).

Table 5.1: The ranges of the scattering curve used per specimen

sample	Steel 10CrMo9 10	Al-6013 3.3 785	Al-6013 3.3 283 10keV and 20keV		Al-2024 & 6013 undef	Al-6013 air	Al-6013 NaCl	Al-2024 CT
range*	40-175	50-175	40-350	40-350	40-350	40-360	40-360	40-250

*The range is given in channels, 365 in total; 283 and 785 stand for the sample thickness in µm;

For the Al-6013 sample, 283µm thick, measured at 10 keV, a damage zone similar to that observed for the total intensity and anisotropy parameters can be discerned (Figure 5.16a), though the value of the fractal dimension parameter n is lower in this region. The undeformed sample also shows these lower values (Figure 5.16b) and the results therefore remain somewhat ambiguous, though as mentioned before, the undeformed specimen is somewhat thinner. On the whole, the value for the fractal dimension parameter n lies between 2 and 3 which points to scatterers showing a fractal structure of type mass or volume.

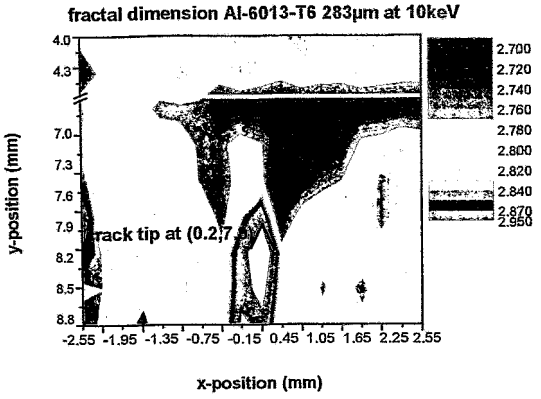

Figure 5.16a: the fractal dimension n for each scan point for the 283µm (at 10 keV) Al-6013 sample shows A damage region of lower values ahead of the crack tip.

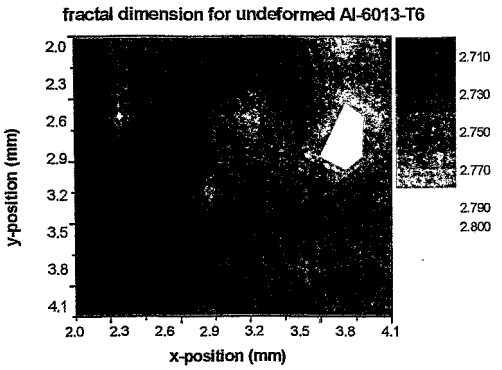

Figure 5.16b: the fractal dimension n for the undeformed Al-6013 sample (at 10 keV) reveals no pattern, but similar values.

At 20 keV, the fractal dimension shows a damage zone similar to those observed from the intensity and anisotropy parameters (Figure 5.17). The value of n is higher for the region immediately ahead of the crack tip.

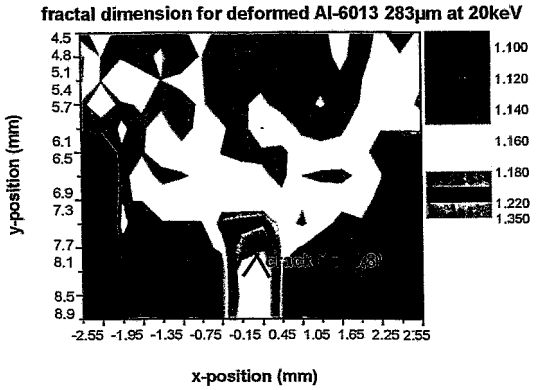

Figure 5.17: the fractal dimension n for each scan point for the 283µm (at 20 keV) Al-6013 sample shows a clear damage zone ahead of the crack tip.

For the thick, 785µm sample, measured at 20 keV, a damage zone ahead of the crack on the left can be seen (Figure 5.18a and b), which corresponds to the region obtained from the anisotropy parameter and in position also corresponds with the integral intensity parameter. On the whole, the value of n lies between 1 and 2, thus is lower for the specimens measured at 20 keV than for those, measured at 10 keV. Choosing a slightly different range, from 56-360 channels for the 283µm Al-6013 sample, does not significantly change the values for n. This leaves only the variables: thickness of the sample, transmission and differences in the scattered intensity.

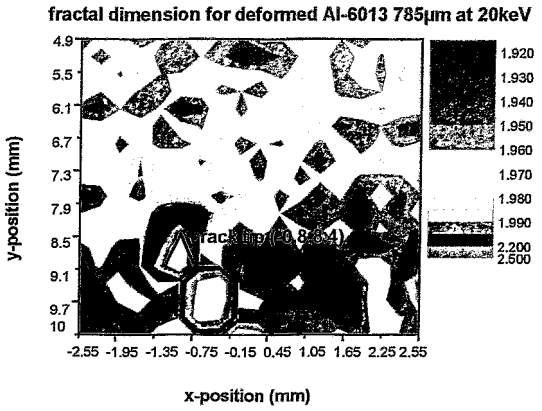

Figure 5.18a: the fractal dimension n for each scan point for the thick 785µm Al-6013 sample. shows a small or large but scattered damage zone ahead of the crack tip.

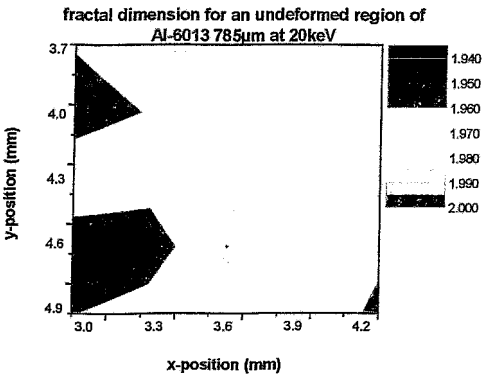

Figure 5.18b: the fractal dimension n for an undeformed region of the sample shows no pattern, but comparable values.

The result for the steel SEN(B) sample after plotting the fractal dimension parameter for each scan point is given in Figures 5.19a and b. A very clear damage zone is observed around the crack tip in Figure 5.19a, while the undeformed region (Figure b) has values clearly below the higher values of the region around the tip. The value of n also lies between 1 and 2.

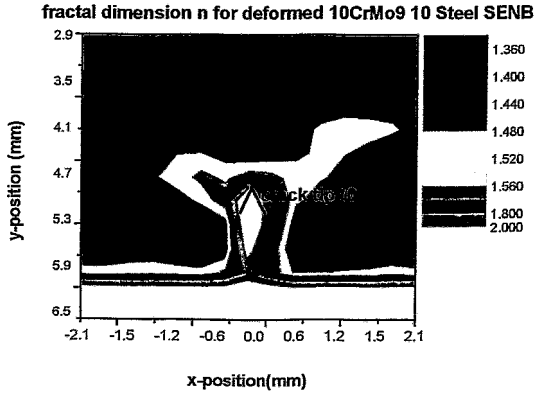

Figure 5.19a: the fractal dimension n for each scan point for the deformed steel SEN(B) sample shows a clear damage zone ahead of the crack tip.

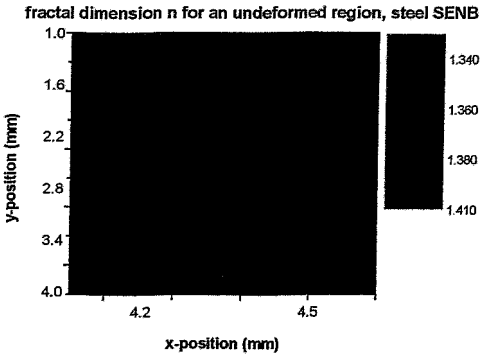

Figure 5.19b: the fractal dimension n for the undeformed region of the steel sample shows no pattern and lower values.

The values of the fractal dimension n for all our specimens, lie between 1 and 3. This implies that the scatterer we are seeing here can be described by a mass or volume fractal structure. It is possible to consider the dislocation patterns to be expected as a result of the deformation and also void structures as strongly irregular or fractal [HAU]. The scattering curves of the crack itself, probably dominated by scattering off the crack edges tend to show values of n between 2 and 3, usually very close to 3 at 10 keV as well as at 20 keV. The value of n=3 represents line dislocations, or of course a linear type of defect such as the transition between the material along the crack or near the edge of the sample and the void of the crack or beyond the sample, and thus gives credence to the proposition that the high intensity regions at the crack are related to scattering off the edges.

A difficulty, however, still exists. From the literature [HAU], the determination of the factor n by which the scattered intensity falls with the scattering vector can easily be carried out for

the asymptotic range of the scattering curve. At 10 keV, the linear range is very wide for all the samples indicating that a valid determination of the fractal dimension is possible. For the thicker Al-6013 sample and for the steel sample at 20 keV, however, the asymptotic part deviates into a second linear tail (Figure 5.15, q=0.65-1 nm^{-1}) which does not visualize a damage zone whereas the fitted range does. This part, however, roughly covers the q-range which is not observed at 10 keV. The q-range covered is, furthermore, wide enough ~1 order of magnitude, as recommended for a valid determination of the fractal dimension [SAS]. It is therefore considered valid to choose the ranges given in Table 5.1 for the determination of the fractal dimension.

The changes in the scattering curve shape over the whole q-range, seen by means of a log-log visualization, can be looked at by plotting the variation of the log-log plot from a linear shape, characterized by the value of χ^2 *(chi-squared)* over the whole range of the scattering curve. If the data correspond to a linear function and the deviations are Gaussian, then the standard deviation should follow a chi-square distribution. The value of χ^2 gives an idea of the goodness of fit. This led to very similar results for the damage zone as obtained for the fractal dimension (Figures 5.19.c and d) and tells us that the scattering curves from scan points corresponding to higher χ^2 values are closer to a linear dependence than those which represent lower values. The χ^2 values were obtained using the whole q-range (40-360 channels).

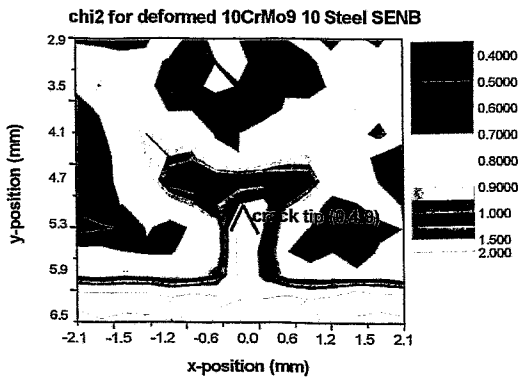

Figure 5.19c: the χ^2-parameter for each scan point for the deformed steel SEN(B) sample shows a damage zone ahead of the crack tip.

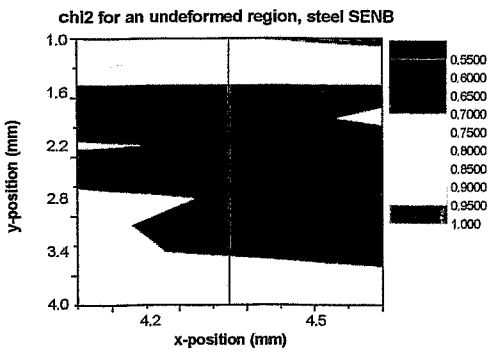

Figure 5.19d: the χ^2- parameter for the undeformed region of the steel sample shows no pattern and lower values.

5.1.5 A damage-related scattering curve?

From the anisotropy, we learned that the material in the undeformed state contains an anisotropic scatterer and that in the region of the crack tip, this anisotropy was changed. It looked like an second anisotropic scatterer was present in the region around the crack tip.

Based on the method used in SANS datahandling to subtract the scattering in the unirradiated material from the scattering in the irradiated material, we here attempted to subtract the scattering observed in the undeformed region from the scattering in the region of the crack tip. As a preliminary test procedure, the scattering data from the undeformed region were averaged and subsequently subtracted from the data around the crack. Figure 5.20 shows a comparison between scatter curves from a scan point: away from the crack (h02 60), near the crack tip (h02 99), from the undeformed (ud) region (h03 11), the average of the undeformed region (avgud), the difference between the scatter curve away from the crack and avgud (I-avgud h02 60), the difference between the scatter curve near the crack tip and avgud (I-avgud h02 99) and the background.

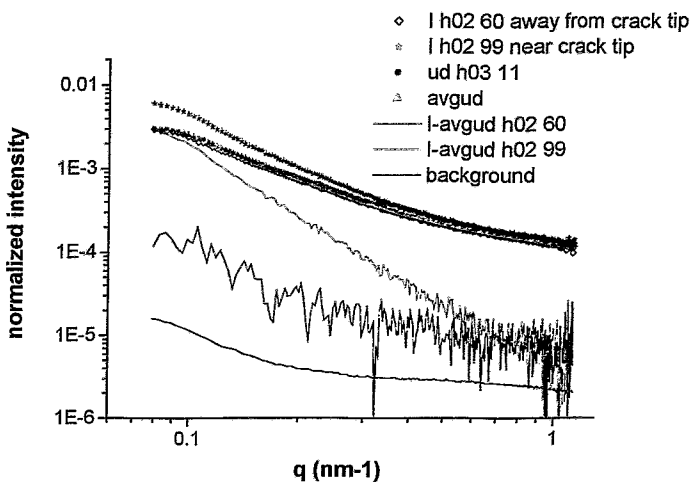

Figure 5.20: comparison of logarithmic scatter curves for the steel sample.

The scan points away from the crack region (h02 60), from the undeformed region (h03 11) and the average (avgud) can hardly be distinguished from each other. The difference between the remainder after subtraction of the averaged undeformed data for the scan point away from and near the crack tip is quite large, though a lot of scatter can be seen for the point away from the crack. The background remains lower. It was therefore attempted to visualize these differences by plotting the anisotropy and fractal dimension parameters (Figure 5.21 and 5.22, respectively). The damage zone can be recognized, especially using the anisotropy, but no further information can be obtained. The values for the fractal dimension still lie between 1 and 2. Immediately around the tip they lie around 2 and above which indicates the presence of spherical shells (n=2), but the values vary widely around 2 and are found as well in the top region of the scan. It is recommended, however, that these results, the scatter curves after subtraction of the averaged scatter curves from the undeformed region, should be investigated in detail, through modelling with e.g. dislocation-like structures.

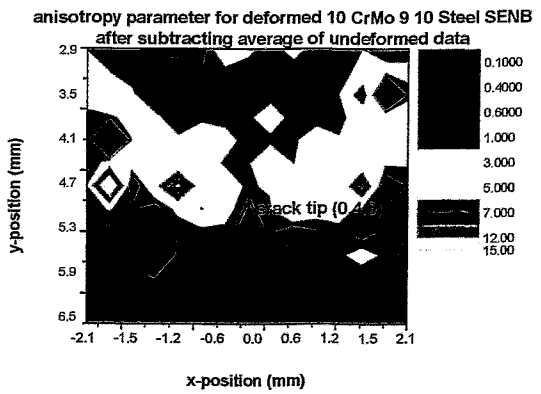

Figure 5.21: the anisotropy parameter after subtraction of the average of the undeformed region Still reveals a damage zone ahead of the crack tip.

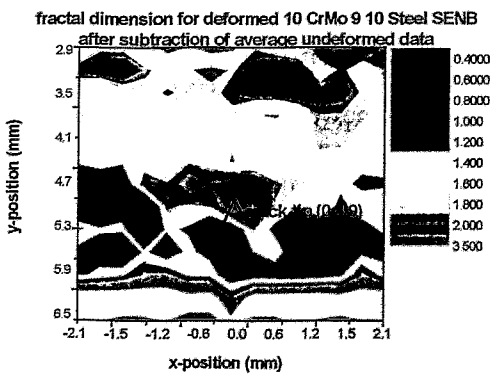

Figure 5.22: the fractal dimension after subtraction of the average of the undeformed region shows a scattered damage zone.

5.2 DISCUSSION

In the following paragraphs, the integral and total intensity, the anisotropy parameter and the fractal dimension parameter results are discussed.

5.2.1 The integral and total intensity parameter

The integral and total intensity in many cases reveal a damage zone, but not in all cases which makes the use of these parameters less than optimal. This is thought to be due to the large amount of scatterers present in the undeformed state which contribute to the overall scattered intensity. In favour of these parameters, though is the fact that the path of the crack can be followed accurately. In the case of the thick 785μm Al-6013 sample, two cracks were observed and a damage zone was observed where other parameters did not see anything. This is not well understood and more data are required to substantiate and explain the observations.

5.2.2 The anisotropy parameter

The anisotropy parameter, is very robust. It is sensitive to a specific anisotropy in the scattering which is clearly related to the deformation-induced damage. It is robust against corrections for the transmission, background and decay of the primary beam intensity. All the specimens showed a clearly defined damage zone.

Figures 5.10a and 5.11a reveal a strong anisotropy with increased scattering parallel to the crack, less pronounced in the latter, but present. Figure 5.14a, does not clearly show this anisotropy and shows values for the anisotropy parameter around 1.

After comparing all the samples, the Al-alloys and the steel sample, we found that the anisotropy is related to the rolling direction of the sheet and plate material. Yet, for the SEN(B) steel sample, the anisotropy was less pronounced and different in shape than for the aluminium M(T)-sheet specimens. This was observed also for the Al-2024-T351 SEN(B) specimen, measured at BW4 at HASYLAB. The anisotropy, therefore seems to be related to the production procedure of the sheet and plate material and the type of deformation, tension or three-point bending in connection with the different thicknesses 1.6mm and 10mm, respectively of the specimens.

Around the crack tip, however, additional scattering is present in a direction transverse to the crack for both aluminium specimens (4.4 and 3.3). In real space, this means that a stretched scatterer in a direction parallel to the crack is present around the crack tip after deformation, which is absent in the region far from the crack tip. For the steel sample, the scattering lies in the opposite direction, parallel to the crack implying a stretched scatterer in real space lying transverse to the crack.

It is well known that for the Al-2024-T351 alloy [ALT] particles may be sheared by dislocations during deformation processes; this is clearly seen in Figure 5.23 made by means of SEM at the university of Halle-Wittenberg, no cracking of the InterMetallic Phases (IMP) was found for the undeformed material.

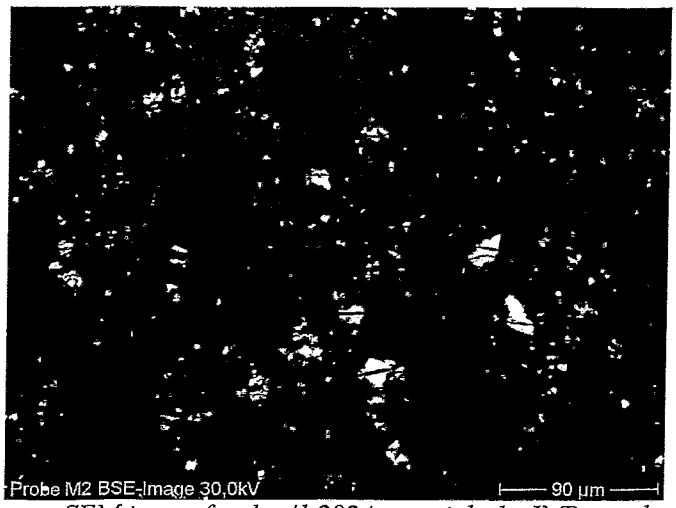

Figure 5.23:Backscatter SEM-image for the Al-2024 material; the IMP are clearly cut through the centre.

The different phases were found to be AlFeMn, Al_2Cu and Al_2CuMg, the latter containing Mg were preferably found inside the grains and smaller than the other phases, while the Al_2Cu were found at the grain boundaries, the AlFeMn were found as well in as at the grain boundaries. This implies, though, that these phases represent hardly any contrast, with the Al –matrix including Cu and Mg and thus should not be visible in the small angle scattering. Care is, however, needed, because the smaller particles are still too big to be observed by means of SAXS. Especially the Al-2024-T351 has been well characterized in the literature, though, and the Al-6013-T6 is being investigated extensively. In the Al-2024 material held at room temperature, coherent Cu and Mg Guinier-Preston zones on {100}-planes with an average diameter of 2 nm and Guinier Preston zones of coherent cylinders in the [100] direction containing Cu of length 4-8 nm were observed [TEM, MER, GOT]. Thus, small coherent particles/zones containing Cu and/or Mg are present in the material, but their contrast with the matrix is expected to be minimal.

It is therefore concluded that the stretched scatterers are unlikely to be the particles themselves. A thought came to mind that the space created as a result of the cracking may be responsible, but the dimensions given on the photograph above are too big.

At this stage, the origin of the scatterer is still unclear and the scattering curves are very complicated and expected to entail a distribution of shapes and sizes. Perhaps, though, some basic assumptions can be made to narrow down the possible scatterer.

As a result of the deformation, immediately ahead of the crack tip, nano- and micro-voids are expected to nucleate, subsequently grow and coalesce, causing crack growth. We do not, however, expect to see these over a wide range around the crack tip. Furthermore, the anisotropy present in the undeformed regions of the samples is used to assess the anisotropy induced after deformation which shows a relationship between the two. From these considerations, knowing that large dislocation networks are already present in the undeformed material after rolling and that large dislocation networks are created as a result of deformation, it is considered very probable that dislocation networks are responsible for the scattering observed. An oriented large dislocation network was observed by means of TEM (Figure 5.25).

Similar considerations should apply to the steel sample for which the enhanced scattering anisotropy in the direction parallel to the crack could find an explanation in the different type of deformation.

5.2.3 The fractal dimension parameter

A clear damage zone ahead of the crack tip can be observed from the visualization of the fractal dimension parameter for the scan region for all specimens. The results correspond reasonable well with the results for the anisotropy parameter. The value of the fractal dimension n lies between 1 and 3 which points to mass (or volume) fractals. As mentioned earlier, dislocation networks may be described as structures of fractal nature.

A linear fit of the log-log plot of the scattering curve I(q) limited to the q-range from ~0.65-1 nm^{-1} for instance for the steel specimen (Figure 5.15) does not reveal any damage region. The region corresponds to the region outside of the 10 keV range and shows that the deformation-related scatterer for these samples is larger than ~10nm; this indicates that the reason why the integral intensity in Figure 5.2a did not reveal a damage zone ahead of the crack tip probably indeed lies in the sensitivity of this parameter to other types of scatterers.

The results show that the fractal dimension parameter is a reliable parameter which provides an idea of the structure of the scatterers. Many questions are still open: the difference in the value of n for the samples measured at 10 keV and 20 keV, the lower n values for the damage zone observed in Figure 5.16a and the fact that the values for n for the damage region lie within the same range as those for the undeformed region for Figures 5.16a,b and 5.18a,b. These questions need to be addressed and would merit further research.

5.2.4 The compact tension (CT) Al-2024-T351 specimen

Figure A.2a reveals a plot of the anisotropy parameter for a specimen cut from a thick CT-specimen. Vaguely a damage zone can be distinguished, but the values corresponding to an undeformed region of the specimen, Figure A.2b, are too high too make any accurate statements on a zone, only light green and yellow values rise above those for the undamaged material, though a truly undeformed specimen was not available and some deformation may be present for the region in Figure b as well. The reason for the patched shaped may lie in the fact that this specimen revealed a much larger grain size, around 70μm by 200μm which meant that the typical anisotropic streak-like scattering characteristic for grain boundary scattering, which was indeed observed, presented a disturbing influence. From this result, it is proposed that to investigate scatterers related to a damage zone other than grain boundaries, the beamsize should either be very small in comparison with the grain size or much larger.

For the integral and total intensity and for the fractal dimension parameters only patched regions of higher parameter values were observed (Figure A.2c and d).

5.2.5 Results from BW4 at HASYLAB

At BW4, the beam intensity was lower and the beam size correspondingly large, about 0.4mm by 2mm. The total intensity does not provide clear images resembling a damage zone as observed before. The anisotropy parameter does, however, and some parts do show correspondence in the total intensity. For the SEN(B) Al-2024 sample (Figures A.7a), the damage zone seems to lie immediately ahead of the crack tip, is thin and stretched and confirmed by the image from the total intensity (Figure A.7b). Figure A.4a reveals the anisotropy parameter for the Al-3.2 sample which was deformed to a comparable extent as specimen 3.3. The damage zone measures around 3mm by 3mm, smaller than expected, but clearly visible. All samples were of approximately equal thickness (Table 3.3) and the scans for the undeformed samples shows values corresponding to those obtained for the region surrounding the damage zone. Specimens 11.1 (Al-2024) and 10.7b (Al-6013) were subjected to different deformation parameters, larger starter notch, much smaller fatigue crack length and slightly smaller crack extension (Table 3.2a). For the Al-2024 material, the damage zone is smaller for specimen 11.1 (Figure A.5a), but for the Al-6013 material, the zones are comparable in size (Figures A.4a and A.6a).

These measurements were still preliminary, it would be interesting to investigate the materials in three different deformation states, or still better during deformation (in-situ).

5.2.6 Finite Element Analysis

The size (~3 mm x 6 mm) and shape obtained from the anisotropy parameter and from finite element calculations, Figures 5.10c and 3.5 respectively, correspond very well. For the Al-6013-T6 specimen 3.3, the correspondence is equally good, Figures 5.11b and 3.5b; the damage zone seems to be slightly smaller, closer to 3mm by 5mm also earlobed, but not as strongly caved in. Figures 5.12 and 5.13a show the anisotropy parameter for the same (3.3) specimen, at a different energy, and for a thicker sample, respectively and Figure A.4a shows that for a similar sample (3.2). The damage zone in Figure 5.11b seems more stretched, but part of the data is missing in the region where the damage zone is expected to be broader. Roughly, the shape and size of the damage zones correspond well with those calculated.

5.3 SUPPORTIVE INVESTIGATIONS

In support of the SAXS-experiments, investigations into microstructural changes near the crack tip and farther from it were carried out using electron microscopy, X-ray diffraction and positron annihilation techniques. These are discussed in the following sections.

5.3.1 Electron Microscopy

Scanning and transmission electron microscopy (SEM and TEM) observations were made. The SEM image revealed a damage zone which was related to differences in grain boundary orientation [POU],[MAR], Figure 5.24 - metallographically no difference in the grain size could be found between the region around and away from the crack tip. From the backscattering SEM-investigations [STI] carried out at the TU-Dresden, no dislocation patterning or networks were observed probably due to the very large networks present which were observed in the TEM (Figure 5.25). Diamond-shaped, round and rod-like (oriented) particles, 10-400nm, were further observed in the TEM (Figures 5.26a and b), but only a tiny region could be imaged and an accurate position of the electron beam with respect to the crack tip could not be given. Further specimens were looked at, but the main information that was obtained from the TEM results is that particles of different shapes and sizes are present in the material which means that modelling of the scattering curve will be very complex involving a size and shape distribution.

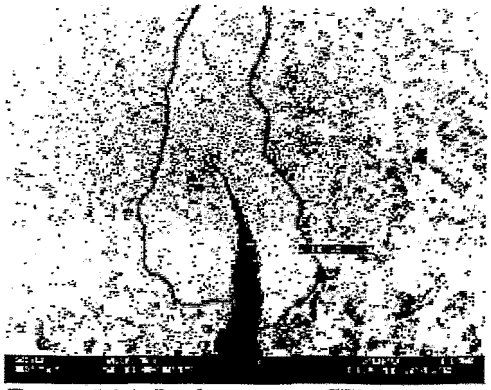

Figure 5.24: Backscattering SEM-investigations revealed a damage zone, around 500μm in width around the crack tip which is related to changes in the grain orientation as a result of the deformation.

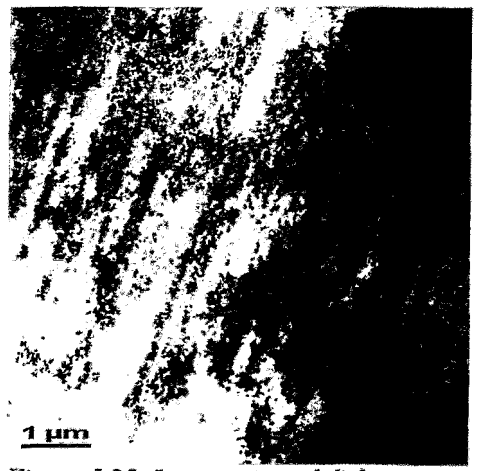

Figure 5.25: Large oriented dislocation networks were observed by means of TEM.

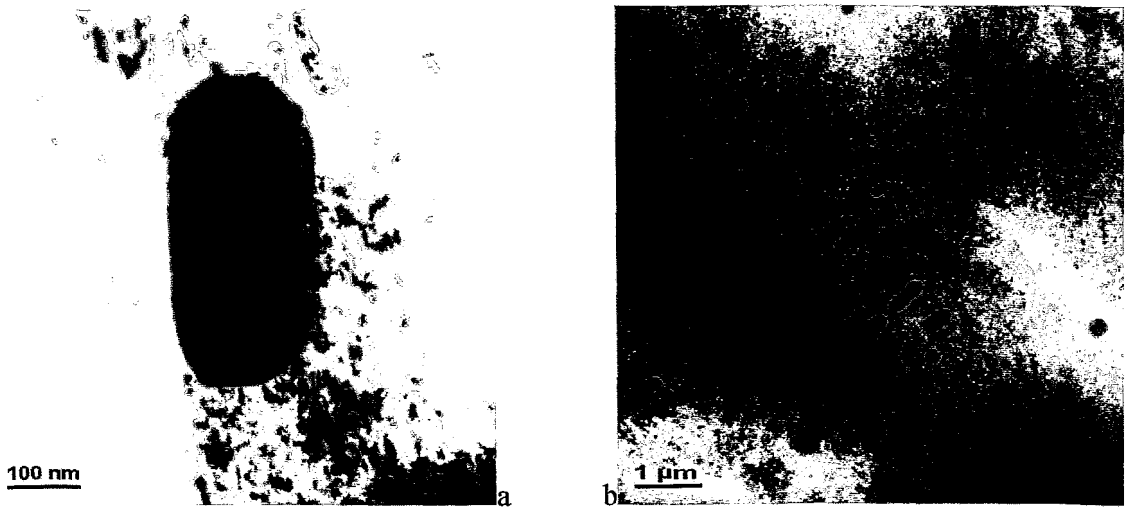

Figures 5.26a and b: Oriented rod-like particles were observed by means of TEM.

5.3.2 X-Ray Diffraction

X-Ray Diffraction (XRD) investigations were carried out at three different locations, at the FZ-Rossendorf, Institute for Ion Beam Physics and Material Research, at the TU-Dresden, Institut für Strukturphysik, former Institut für Physikalische Metallkunde, and at the G3 beamline at Hasylab, Hamburg. The XRD-measurements at FZ-Rossendorf and at the TU-Dresden were carried out, using Cu-Kα radiation. Two measurements were made using a beam of size ~1 mm, one immediately at the crack tip and the other further from the crack tip. Both institutes showed that there was a tendency towards smaller FWHM (Full Width at Half Maximum) and IW (Integral Width) in the crack tip region compared to outside for all reflexes measured (111),(200),(220),(311),(222),(400). The results imply that the effect is related to grain size rather than dislocation networks. The size of the coherently scattering regions seemed to be slightly larger (34 nm) in the crack region than outside (24 nm).

At the G3 beamline at Hasylab, however, synchrotron radiation was used to investigate the material by means of the MAterials X-ray IMaging (MAXIM) technique [WRO,*,**]. This technique allows high resolution diffraction measurements by placing a multichannel plate in front of the detector into the secondary beam. For each channel, corresponding to ~12.5 µm, diffraction data are obtained. With this technique, broadening of the 311-reflex was indeed observed near the crack tip for the Al-6013-T6 alloy, as is shown in Figure 5.27, below.

This may point to extensive dislocation networks around the crack tip, which is known to cause broadening.

Broadening, can, however, also be caused by changes in the grain size. Electrical resistance measurements, carried out at the university of Halle [Schmidt], revealed that the grain size increased with increasing distance from the crack tip, from an average grain size of 25.8µm at the crack tip, to 34.4µm and 53.7µm, the last value near the specimen edge. The specific resistance of the specimens rose with increasing distance from the crack tip, though the opposite was expected. Furthermore, all investigations revealed a high dislocation density in the undeformed material, which is very probably caused by rolling and this has in most case caused difficulties observing any patterning of the dislocations.

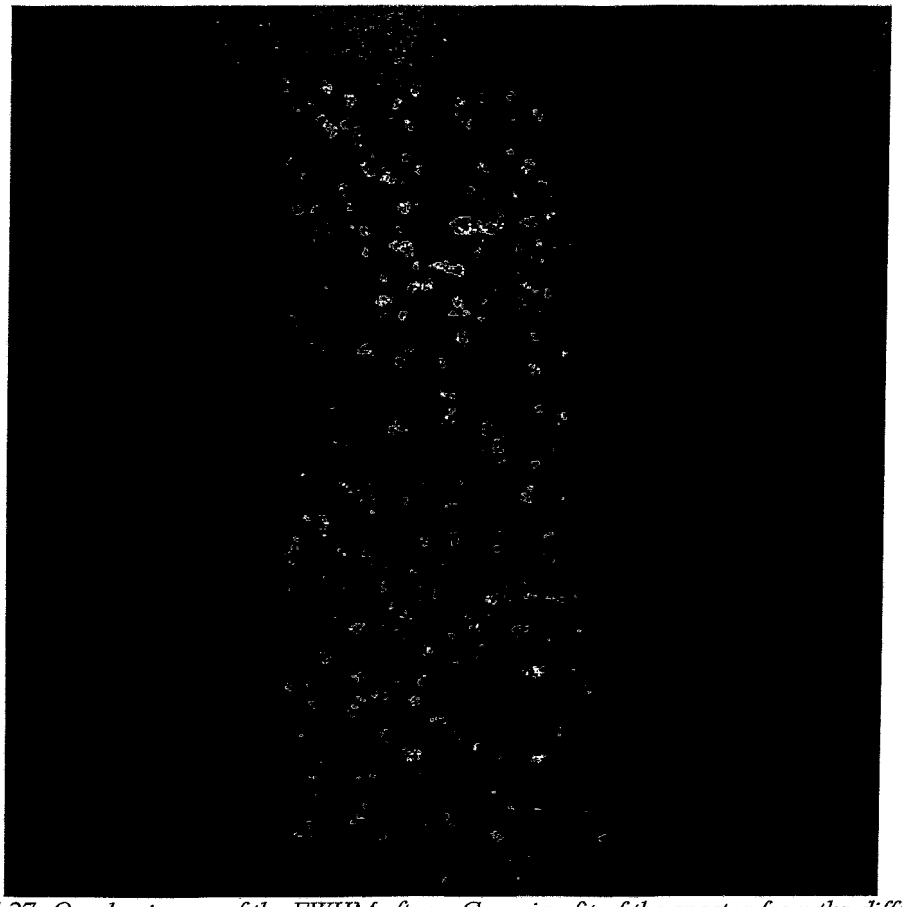

Figure 5.27: Overlay image of the FWHM after a Gaussian fit of the spectra from the diffraction experiments on the image of the grains lying in the orientation of the reflex using the MAXIM technique at the G3-beamline at Hasylab.

5.3.3 The Positron Annihilation Microprobe

At the university of Bonn, Institut für Strahlen- und Kernphysik, the opportunity arose to carry out a test experiment using the Positron Annihilation Microprobe (PAM) [GRE],[HAA] on an Al-2024-T351 sample. This probe is an electron microscope, adapted to be capable of delivering a positron or an electron beam to the sample. Using the electron beam, the sample can be accurately positioned. Subsequently the positron beam can be turned on and focused to a beam size of around 20μm. For a small region of the sample, the s-parameter, a measure of the Doppler broadening of the annihilation radiation can be determined and plotted. Figure 5.28 shows the result. The scan was, however, not completed, yet a small zone immediately ahead of the crack tip shows an increased value of the s-parameter. Only 0.5 mm by 0.5 mm of the sample was scanned and the background value for the s-parameter was not yet reached, implying that the entire zone scanned is part of the damage region around the crack tip as observed for sample 4.4 in Figure 5.10c. The technique seems very promising.

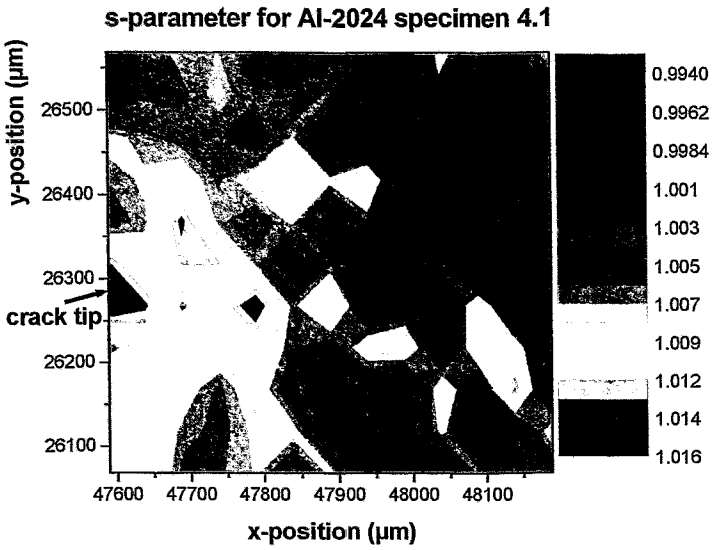

Figure 5.28: the s-parameter reveals a small intens damage zone immediately ahead of the crack tip.

6. Conclusions

Several important steps leading to a method to analyze the damage zone around the crack tip in metals were investigated and described. In short, these are the type of material, the synchrotron source and beamline requirements, data handling and processing and the determination of a robust damage parameter.
The integral and total intensity did not provide reliable results, probably because the definition itself implies that they are sensitive to all small angle scatterers.
The anisotropy parameter provided very reliably robust results which compare well with finite element calculations. It furthermore allowed to limit particular beamline parameters, thus aiding in the development of the method. It is also a very simple parameter and can be determined from the raw data, and does not require prior integration.
The fractal dimension parameter is a robust parameter which provides results which are comparable to those for the anisotropy parameter, it is somewhat less robust and requires more data handling, integration and fitting, but information about the structure (fractal) of the scatterer can be determined.
The anisotropy and fractal dimension parameters are proposed as damage parameters to investigate the damage zone ahead of the crack tip.
From basic considerations, the damage ahead of the crack tip observed with these parameters is suggested to be related to large oriented dislocation networks.

7. Recommendations for further research

The measurements conducted and described in this report were still preliminary. From them parameters were distilled which can visualize the damage zone ahead of a crack tip. Up to now only pre-deformed samples were tested in only minimally changed deformation states. It is recommended in a next step to investigate the materials, each having been subjected to at least three different amounts of deformation. Secondly, SAXS-experiments during in-situ

deformation should be carried out. Facilities are available at DUBBLE, ESRF and BW4, Hasylab.
Parallel to this, experiments of a small region using a microbeam of 5-10 μm by 5-10 μm (ID11 and/or ID13, ESRF) should be carried out.
Thirdly, in this work, we started also to prepare different types of specimens with different cracks, sharp, dull, centred, on the outside, M(T)-type and SEN(B)-type, but have not got very far. To establish a connection between the parameters developed in this work and mechanical parameters, such as the triaxiality (which changes for different specimen and crack geometries), experiments using different specimens and crack geometrie should be continued.

8. References

[ALT]: E.Altstadt, Extension of the ANSYS® creep, plasticity and damage simulation capabilities. FZ-Rossendorf 2003, Dresden, section 4.

[ASTM]: 1999 Annual Book of ASTM Standards, Vol.03.01, ASTM, West Conshohocken, Pennsylvania, E561, E647 and E1290

[BAL]: K.Balewski, W.Brefeld, U.Hahn, J.Pflüger, R.Rossmanith, An undulator at PETRA II – A new Synchrotron Radiation source at DESY, DESY, Hamburg, Germany

[RIC]: Ermittlung zähbruchmechanischer Kennwerte unter schlagartiger Belastung mittels Schallemission. Holger Richter, September 2000, FZR-299, FZ-Rossendorf e.V., Dresden.

[GOT]: G.Gottstein, Physikalische Grundlagen der Materialkunde (2001) Springer-Verlag, 381-382

[GRE]: H.Greif et.al., High resolution positron-annihilation spectroscopy with a new positron microprobe. Applied Physics Letters, 71(15) (1997), 2115-2117

[HAA]: M.Haaks et.al., Measurements on crack tips in stainless steel AISI 321 by using a new positron microprobe. Applied Surface Science 149 (1999), 207-210.

[GRO]: M.Große, J.Böhmert, C.Riekel; J. of Material Science Letters 17 (1998) 1631-1634.

[GRO*]: M.Große, J.Böhmert; 29.DVM Tagung 'Bruchvorgänge', Februar 1997, 299-306.

[GRO**]: M.Große, J.Böhmert; FZR-229, Juli 1998, Forschungszentrum Rossendorf, Dresden.

[HAU]: 23.IFF-Ferienkurs, Synchrotronstrahlung zur Erforschung der Materie, 23.March-3.April 1992, FZ-Jülich, chapter 29, H.-G.Haubold, 12-14

[KRA]: O.Glatter, O.Kratky, Small Angle X-ray Scattering.

[JUE]: Synchrotronstrahlung zur Erforschung kondensierter Materie, 23.IFF Ferienkurs, FZ-Jülich, 1992

[MAN]: B.B.Mandelbrot, Die fraktale Geometrie der Natur (1987) Akademie-Verlag, Berlin, 7-8,27-28

[MAR]: In Situ Measurement of Grain Rotation During Deformation of Polycrystals. L.Margulies et.al., SCIENCE, 291 (2001), 2392-2394

[MER] : M.Merkel, K.-H. Thomas, Taschenbuch der Werkstoffe (2000) Fachbuchverlag Leipzig, 309-

[POU]: Three-dimensional maps of grain boundaries and the stress state of individual grains in polycrystals and powders. H.F.Poulsen et.al., J.of Applied Crytallography, 34 (2001), 751-756

[SAS]: Introductory training in SAXS/WAXS at ELETTRA, Trieste, August 23-24 2002.

[Schmidt]: Private Communication, U.Schmidt, Fachbereich Physik, Martin-Luther University, Halle (March 2003)

[STI]: SEM-ECC Imaging and SAC-Patterns-Procedures for the nondestructive characterization of microstructures and for revealing the global dislocation arrangement. C.Stickler, Prakt.Metallogr.38 (2001)10, 566-590.

[TEM]: Private communication, September 2002, AIRBUS Bremen

[WRO]: A new diffractometer for materials science and imaging at HASYLAB beamline G3. T.Wroblewski et al., Nuclear Instruments and Methods in Physics Research A 428 (1999), 570-582

[WRO*]: X-ray imaging of polycrystalline materials. T.Wroblewski, S.Geier, et al., Ren.Sci.Instrum.66, 6, (June 1995), 3560-3562

[WRO**]: X-ray imaging using the radiation diffracted by polycrystalline materials. T.Wroblewski, Radiation Physics and Chemistry 61 (2001), 329-332

Addendum A. Listing of additional results from DUBBLE and BW4

The results from the fatigued Al-6013 specimens, for the CT Al-2024 specimen and for the specimens measured at BW4, HASYLAB are given below (Table 3.3). The results from the anisotropy parameter for the 4.4 Al-2024-T351, 135μm thick, measured at BW4 at 10.1keV were given earlier.

Fatigued in air and in NaCl specimens Al-6013-T6, measured at DUBBLE at 10keV

Two small specimens about 5mm x 5mm in size, one fatigued in air and the other in NaCl, were also investigated, Figures A.1a,c and b,d respectively. The image resulting from a plot of the anisotropy parameter (a,b) does not reveal a clear damage zone, a higher value for the parameter is observed around the crack tip, but the specimen in air shows very strong scattering along the whole width of the specimen, which is not expected since the specimen was merely fatigued which means that a small damage region of about 300μm by 400μm or even smaller is expected. The specimen fatigued in NaCl, also shows higher values near the upper edge of the specimen, which is also not clear but could relate to scattering of the edge of the sample clamped from the bottom close to the crack. The integral and total intensity show similar patterns, which may indicate that our stretched scatterer is caused by further plastic deformation. Figure A.1c and d both reveal a value of the fractal dimension n between 2 and 3, but no clear damage zone. This may relate to dislocation networks described as mass fractals. This is plausible if one considers that the material in its undeformed state already contains a large amount of dislocations as a result of the rolling treatment.

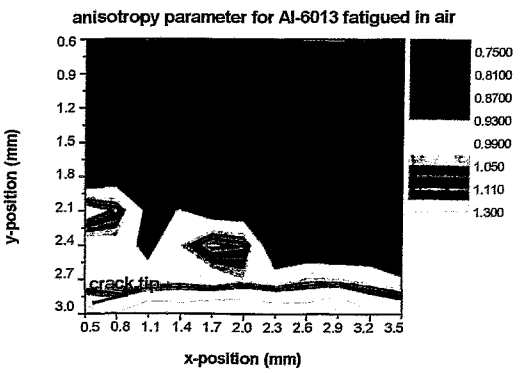

Figure A.1a: the anisotropy parameter for Al-6013 fatigued in air at 10keV.

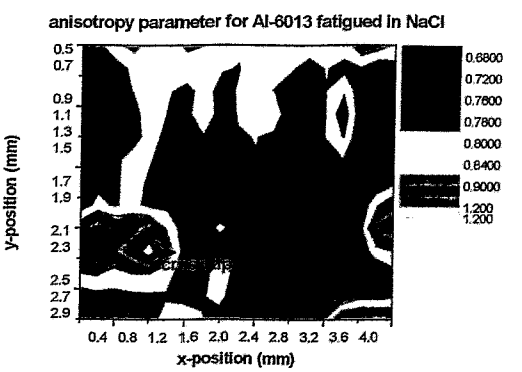

Figure A.1b: the anisotropy parameter for Al-6013 fatigued in NaCl at 10keV.

Similar images are obtained for the integral and total intensity parameters.
No damage zone can be recognized.
The fractal dimension parameter n over the larger part of the scanned region for both samples displays values around n=2.7. Only at the edges, the values differ; this is most likely related to scattering of the edges. For the specimen, fatigued in NaCl, Fig.A.1d, the crack itself is clearly visible.

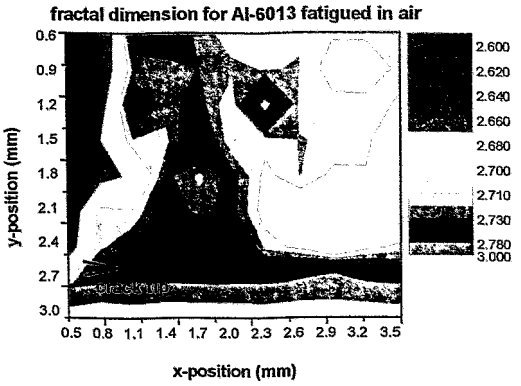

Figure A.1c: the fractal dimension for Al-6013 fatigued in air at 10keV.

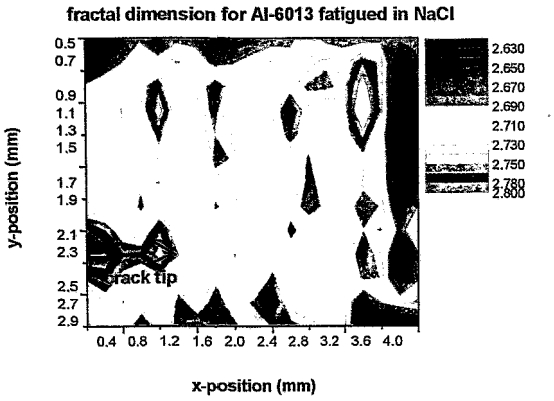

Figure A.1d: the fractal dimension for Al-6013 fatigued in NaCl at 10keV.

Specimen CT Al-2024-T351, measured at DUBBLE at 10keV

Only the anisotropy parameter seems to reveal a region which looks like the damage shape expected, but this is not beyond doubt, since the background value are high. The difficulty visualizing the damage around the crack tip is probably related to the anisotropic interference from grain boundary scattering.

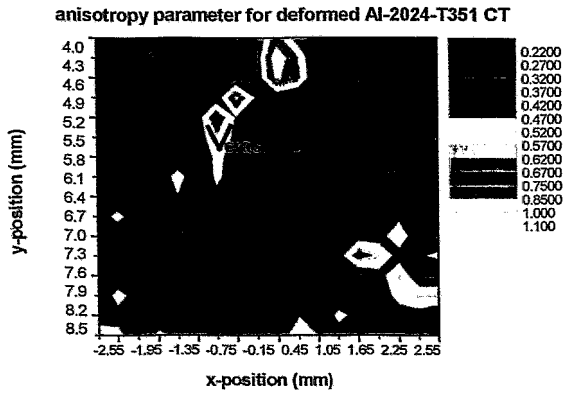

Figure A.2a: the anisotropy parameter for the deformed CT Al-2024 specimen at 10keV.

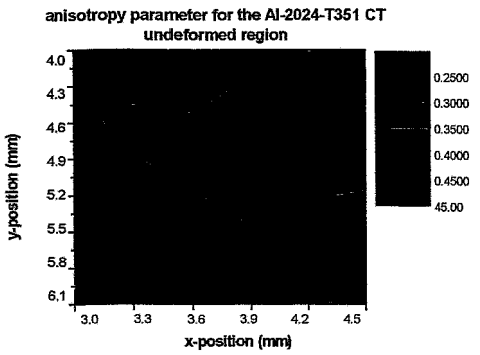

Figure A.2b: the anisotropy parameter for the CT Al-2024 undeformed region at 10keV.

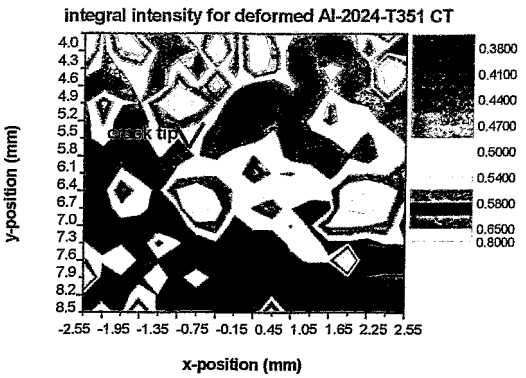

Figure A.2c: the integral intensity for the deformed CT Al-2024 specimen at 10keV.

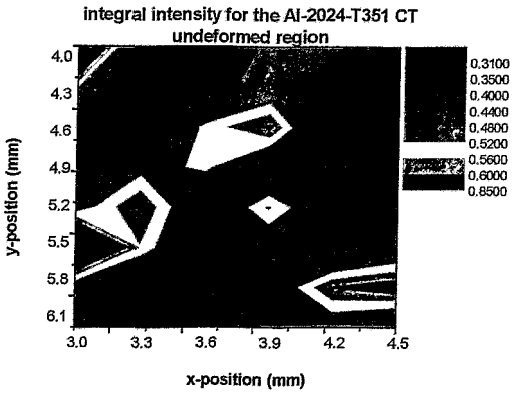

Figure A.2d: the integral intensity for the CT Al-2024 undeformed region at 10keV.

Similar results were obtained for the total intensity and fractal dimension parameters.

The anisotropy parameter for the specimens investigated at BW4 is shown on the following pages.

Specimen 4.4 Al-2024-T351, measured at BW4 at 10.1keV

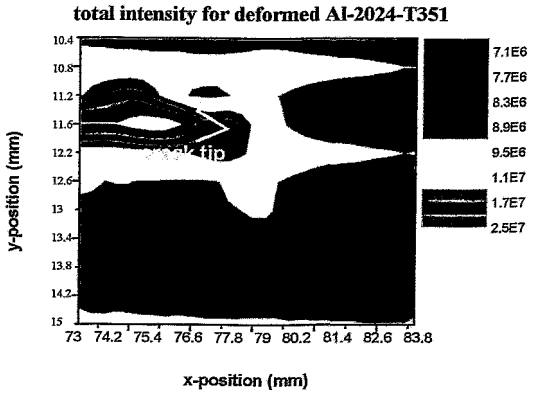

Figure A.3a: the anisotropy parameter for the deformed 4.4 Al-2024 specimen at 10keV.

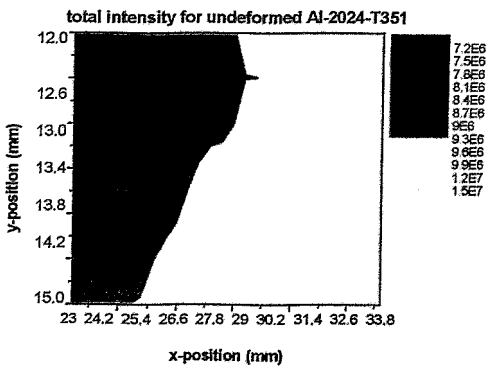

Figure A.3b: the anisotropy parameter for the undeformed Al-2024 specimen at 10keV.

Specimen 3.2 Al-6013-T6, measured at BW4 at 10.1keV

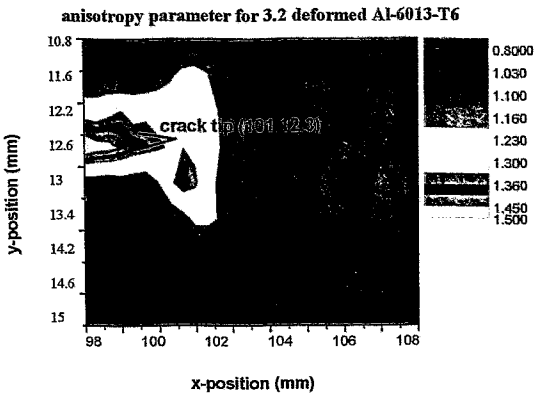

Figure A.4a: the anisotropy parameter for the deformed 3.2 Al-6013 specimen at 10keV.

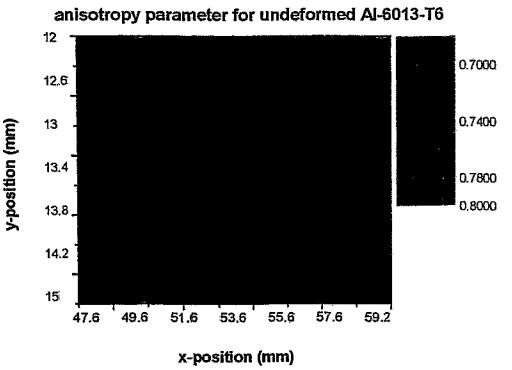

Figure A.4b: the anisotropy parameter for the undeformed Al-6013 specimen at 10keV.

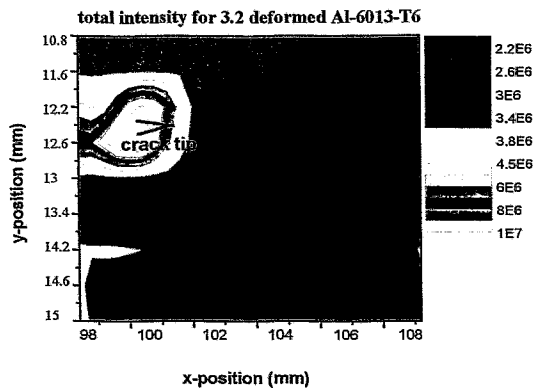

Figure A.4c: the total intensity for the deformed 3.2 Al-6013 specimen at 10keV.

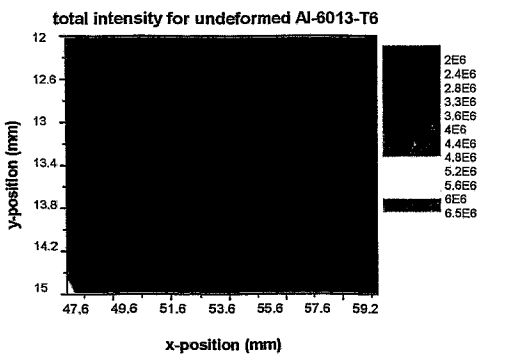

Figure A.4d: the total intensity for the undeformed Al-6013 specimen at 10keV.

Specimen 11.1 Al-2024-T351, measured at BW4 at 10.1keV

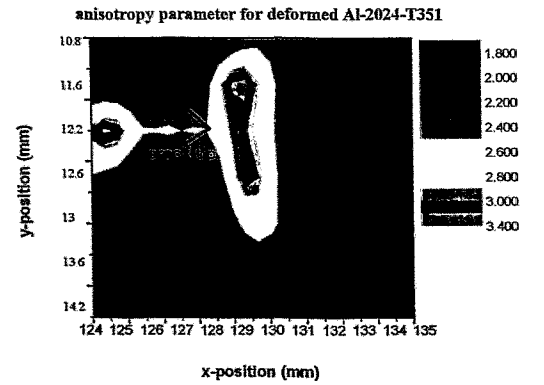

Figure A.5a: the anisotropy parameter for the deformed 11.1 Al-2024 specimen at 10keV.

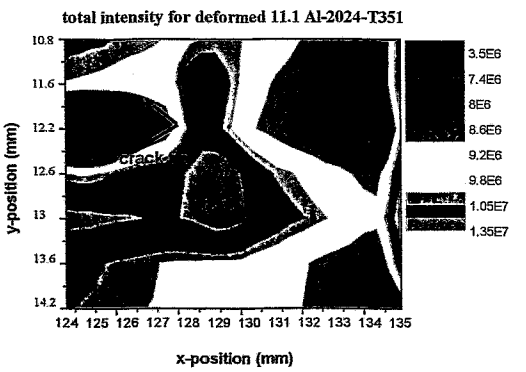

Figure A.5b: the total intensity for the deformed 11.1 Al-2024 specimen at 10keV.

Specimen 10.7b Al-6013-T6, measured at BW4 at 10.1keV

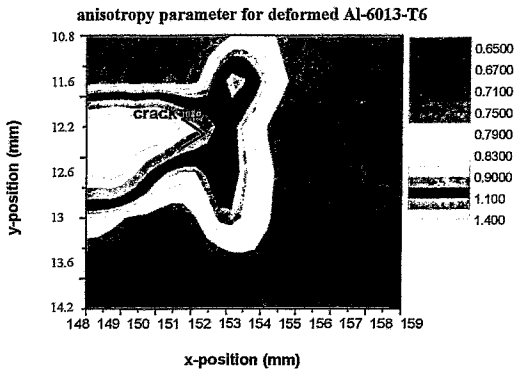

Figure A.6a: the anisotropy parameter for the deformed 10.7b Al-6013 specimen at 10keV

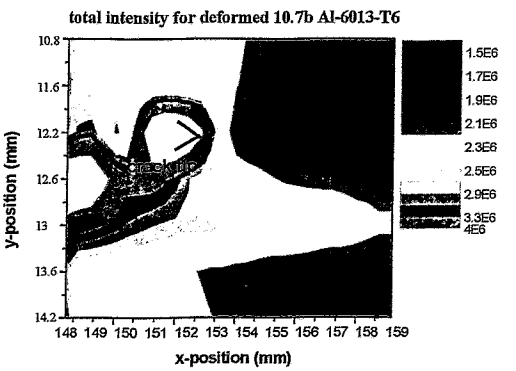

Figure A.6b: the total intensity for the deformed 10.7b Al-6013 specimen at 10keV

Specimen SEN(B) Al-2024-T351, measured at BW4 at 10.1keV after a slight deformation in three-point-bending.

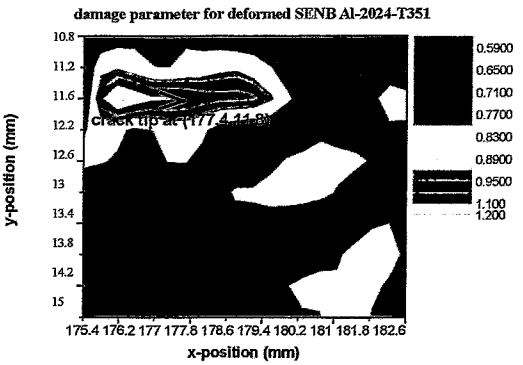

Figure A.7a: the anisotropy parameter for the deformed SEN(B) Al-2024 specimen at 10keV.

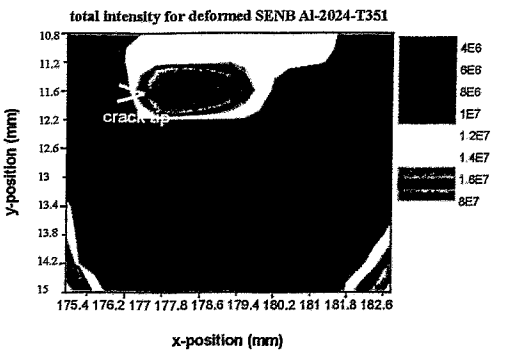

Figure A.7b: the total intensity for the deformed SEN(B) Al-2024 specimen at 10keV.

Addendum B. Determination of uncertainties

In the addendum some errors and uncertainties are listed and explained including basic error propagation.
Figures B.1a and b reveal that the I(q) scattering curves for two scan points from the steel sample and for three scan points on an Al-alloy sample correspond excellently. This proves that the error made by correcting for background and transmission only after azimuthal integration when determining the integral intensity and fractal dimension parameters is negligible. This option was chosen to simplify data handling.

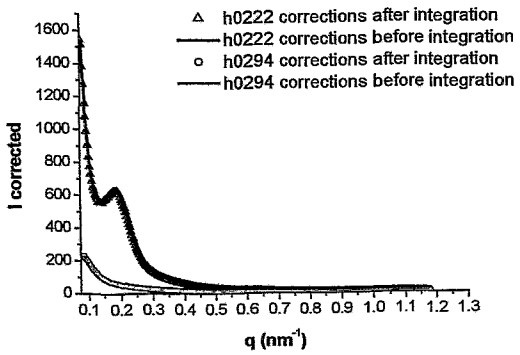

Figure B.1a: Comparison of the I(q) scattering curves obtained applying corrections before and after the azimuthal integration for scan points h0222 and h0294 on the steel specimen in the region of the crack.

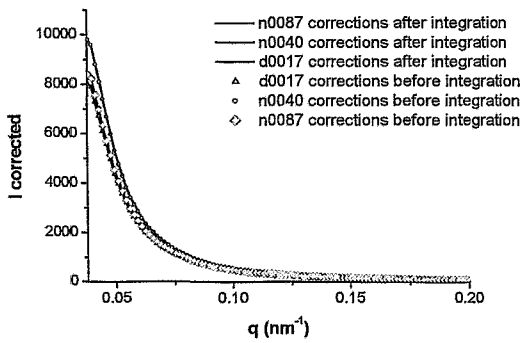

Figure B.1b: same as B.1a for scan points n0044 and 87 and d0017 on the 283μm thick Al-sample at 10keV.

The following table lists the parameters involved in the analysis of the data (DUBBLE) and their estimated systematic and random errors. The systematic errors lie mainly in the settings of the apparatuses and components used and in the fact that usually one experimenter carries out the calibration. These errors are not very well known, but considered negligible in what follows. Many settings and sample mounting were carried out together, which minimizes the one-person influence on a systematic error. In addition, the randoms errors from analysis and experiment are considered to be greater.

parameter	error	remarks
beam centre	1 channel	
wavelength	6E-5 nm	spectral bandwidth $\Delta\lambda/\lambda \sim 5x10^{4}$
sample-detector distance		calculated from rat's tail calibration
detector efficiency		variations in the response over the detector area lie between 0.5 to 1.5 (intensity)
duration of the illumination	1 ms	detector dead time = 1 ms
ion chamber efficiency		
motor position	1 μm	reflects the accuracy of sample position

The use of a beamstop, a high synchrotron flux and accurate setting of the guard aperture allow us to minimize scattering off the primary aperture. The remaining influence is corrected for by subtracting the background. The detector dark current is random; it was estimated to be around an average of 10 counts/s which is very small and is generally neglected.
The background and primary intensity decay are corrected for using the following normalization:

$$I_{corrected} = \frac{I_{measured}}{ion2} - \frac{I_{background}}{ion2_{background}}$$

On the right-hand side of the equation, the correction trmisfactor=1.016, 1.005, 1.024 for B0*, C0*-D0* and G0*-H0* bsl/otoko files respectively, can be omitted when normalizing (otherwise multiplied with right-hand terms) because it is constant for both terms on the right. To avoid normalization (especially thinking of determining the actual integral intensity), tests were carried out for all parameters by simply multiplying the background values with the transmission (ion2/ion1). Similar results were obtained, except for the cases where a refill of the ring took place in which case the correction for the primary beam I_0 decay is necessary.

The uncertainty (ΔA) on the values for the anisotropy parameter (A) are estimated on the basis of the following considerations using the more conservative simple average error propagation method.

$$A = \frac{\sum I_{vert}}{\sum I_{hor}} \quad \text{and} \quad I = \frac{I_{measured}}{ion2} - \frac{I_{background}}{ion2bkg}$$

then $$\Delta I = \Delta I_{measured}\left(\frac{1}{ion2} + \frac{1}{ion2bkg}\right) + \frac{1}{2}\Delta ion2\left(\frac{I_{measured}}{ion2^2} + \frac{I_{bkg}}{ion2bkg^2}\right)$$

where $\Delta I_{measured} = \Delta I_{background}$ and $\Delta ion2 = \Delta ion2bkg$ and $\Delta I_{measured} \approx 52$

ΔA is expected to be 0.005

The uncertainty (Δq) for the scattering vector q is determined from the uncertainty on the rat's tail collagen d-spacing.

Addendum C. Data-handling

In the following, a schematic diagram (Figure C.1) is shown which visualizes the data-handling steps. Table C.1 lists the programs that were written in IDL. They will remain accessible on the intranet. An example of a macro written in Fit2D and a few examples of programmes written in IDL: dampardub.pro, dampar.pro and linfitdub.pro are given.

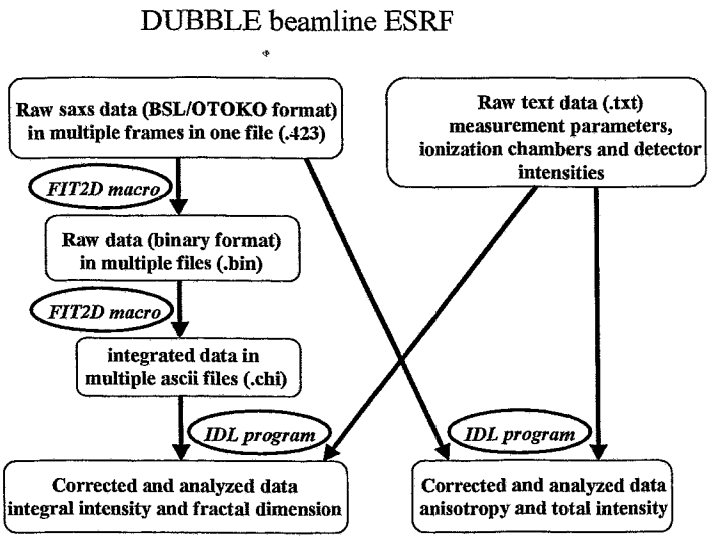

Figure C.1: a schematic diagram shows the basic data-handling steps from the raw saxs-data collected on the detector and the measurement parameter and ionization chamber data to the determination of a damage parameter.

The table below lists the programs that were written in IDL to perform basic data handling and developing the different damage parameters.

Table C.1: Programs in IDL

Program name	Short description
dampardub.pro	determines the anisotropy parameter from the binary and text files from DUBBLE
iidub.pro	determines the integral intensity from the ascii (after azimuthal integration using FIT2D) and text files from DUBBLE
totidub.pro	determines the total intensity from the text files from DUBBLE
linfitdub.pro	determines the fractal dimension from a linear fit from the ascii (after azimuthal integration using FIT2D) and text files from DUBBLE
subtractuddub.pro	determines the fractal dimension after subtraction of the averaged undeformed data
anissubuddub.pro	determines the anisotropy parameter after subtraction of the averaged undeformed data
dampar.pro	determines the anisotropy parameter from the binary and text files from BW4
dampartoti.pro	determines the total intensity from the binary and text files from BW4

The macro 'dubazint.mac' (for 10keV) runs under FIT2D for Windows written by Andy Hammersley, ESRF. It reads in the raw data (.bin) files and integrates along the azimuth and produces the .chi files containing I(q). In FIT2D go to MACROS, then RUN SEQUENCE and **1.**give name of macro: dubazint.mac, **2.**first file of the sequence, then **3.** last file of the sequence, then the macro will run.

```
%!*\ BEGINNING OF GUI MACRO FILE
%!*\
%!*\ This is a comment line
%!*\
EXIT
SAXS / GISAXS                    %! starts the saxs program
INPUT
#IN                              %! reads in the first file, second, ....
X-PIXELS                         %! data parameters
512
Y-PIXELS
512
DATA TYPE
INTEGER (2-BYTE)
SIGNED
NO
BYTE SWAP
YES
STARTING BYTE
1
O.K.
INTEGRATE                        %! go to the integration routine
X-PIXEL SIZE                     %! give detector, wavelength data
260
Y-PIXEL SIZE
260
DISTANCE
8100
WAVELENGTH
1.243000
X-BEAM CENTRE
252.0000
Y-BEAM CENTRE
256.0000
TILT ROTATION
0.0
ANGLE OF TILT
0.0
O.K.
SCAN TYPE                        %! Choose scan type I(q) or I(r) or ...
Q-SPACE                          %! Stands for I(q)
CONSERVE INT.
NO
POLARISATION
YES
FACTOR
0.990000
GEOMETRY COR.
YES
MAX. ANGLE
0.671025
SCAN BINS
365
MAX. D-SPACING
```

```
650.0000
O.K.
OUTPUT
CHIPLOT
OUTPUT ROWS
YES
ROW NUMBER
1
COLUMN NUMBER
1
#OUT
O.K.
EXIT
MACROS / LOG FILE
%!*\ END OF IO MACRO FILE
```

The programs run under IDL (Version 5.4) for Windows.
The program 'dampardub.pro' (DUBBLE) reads in the raw image data corrects them for transmission and background, then determines the ratio of the total intensity over a horizontal and vertical scan of the corrected image data and gives out this result in ascii for the whole scan region.

```
;determine a damage parameter
h=lonarr (1281)
N=25                    ; number of bin files, i changes from 1 to N per file
P=25                    ; number of rows in the txtfile containing 2 columns: ion1, ion2
Ns=1
Nf=25                   ; number of bin files, i changes from 1 to N, Ns to Nf per file
trmisfactor=1.024
bkgfactor=1.2                   ;calibration factor for ion2 wrt ion1
d=uintarr(512,512)                      ;variable containing raw saxs-data
e=fltarr(2,P)                           ;variable containing ascii/txt-data
dvh=fltarr(1,1,N)
dvert=fltarr(1,512)
dhor=fltarr(512,1)
filename='g06'                          ;first 3 or 4 lettres characterizing the filename
folder='33760mu/'                       ;subdirectory or folder of saxs-data
txtfolder='33760mures/'         ;subdirectory or folder of ascii/txt-data
txtfilename='33760mug06.txt'    ;ascii/txt-filename
txtfile=strtrim(STRING(txtfolder),2)+strtrim(STRING(txtfilename),2)
bkgfil='bkgfiles/bkg20kevh04.bin'       ;background filename
 openr,u,bkgfil,/get_lun
 readu,u,d
 BYTEORDER,d
 close,u
 free_lun,u
 w1=float(d)/trmisfactor

 openr,v,txtfile,/get_lun
 readf,v,e
 close, v
 free_lun, v

FOR i=Ns, Nf DO BEGIN

        IF (i GT 99) THEN BEGIN
                addnull='0'
        ENDIF ELSE BEGIN
                IF (i LT 10) THEN addnull='000' ELSE addnull='00'
```

```
        ENDELSE

        filei=strtrim(STRING(folder),2)+filename+strtrim(STRING(addnull),2)+strtrim(STRING(i),2)+'.bin'
        ;datfile=strtrim(STRING(datfolder),2)+filenames(j-
        1)+strtrim(STRING(addnull),2)+strtrim(ST;RING(i),2)+'.dat'
 print,filei
;print,datfile
 openr,u,filei,/get_lun
 readu,u,d
 BYTEORDER,d
 close, u
 free_lun,u

 ion2=e(1,i-1)
 ion1=e(0,i-1)
 ion2=ion2/trmisfactor
 transmis=ion2/ion1

 data=float(d)
 corrdata=data/transmis-w1*bkgfactor
 dvert=corrdata(258:258,0:511)
 dhor=corrdata(0:511,253:253)
 sumdvert=TOTAL(dvert)
 sumdhor=TOTAL(dhor)
 damageparam=sumdhor/sumdvert

 print,damageparam
 dvh[*,*, i-Ns]=damageparam

ENDFOR

openw,uf,'33760mures/pg06.dat',/get_lun
printf,uf,dvh, FORMAT='(5(g0,1x))' ;prints 18 data values horizontally and next 18 below ...
close,uf
free_lun,uf

END
```

The program 'dampar.pro' (BW4-Hasylab) reads in the raw image data, corrects them for transmission and background, then determines the ratio of the total intensity over a horizontal and vertical scan of the corrected image data and gives out this result in ascii for the whole scan region.

```
;determine a damage parameter
h=lonarr (1261)
M=7
N=28
Ns=1
Nf=28
Nt=196
d=uintarr(512,512)
dvh=fltarr(1,1,N)
dvhtot=fltarr(1,1,Nt)
dvert=fltarr(1,512)
dhor=fltarr(512,1)
filenames=['12undef_','12p6undef_','13undef_','13p4undef_','13p8undef_','14p2undef_','15undef_']
folder='ud6013/'
datfolder='ud6013dat/'
```

```
bkgfile='empty/empty220130s.GQE'
 openr,u,bkgfile,/get_lun
 readu,u,h
 readu,u,d
 close,u
 free_lun,u
datbkgd='empty/empty220130s.dat'
 openr,v,datbkgd,/get_lun
  calval=7.49168
  line= ""
  while (not eof (v)) do begin
  readf, v, line
  line= STRTRIM (line,2)
  lengi=strlen(line)
  ionnulbkgfind=strpos(line,'integral intensity I0 per sec')
  if (ionnulbkgfind eq 0) then begin
   ionnulbkg= strmid (line, 33)
   ionnulbkgval=FLOAT(ionnulbkg)
  endif
 iononebkgfind=strpos(line,'integral intensity I1 per sec')     ;not tested
  if (iononebkgfind eq 0) then begin                            ;finds ion1 and turns string
   iononebkg= strmid (line, 33)                                 ;into a floating point value
   iononebkgval=FLOAT(iononebkg)                                ;
  endif                                                         ;

  bsbkgfind=strpos(line,'integral intensity at primary')
  if (bsbkgfind eq 0) then begin
   bsbkg= strmid (line, 50)
   bsbkgval=FLOAT(bs)
   bsbkgvalcal=bsbkgval/calval
   transmisbkg=bsbkgvalcal/ionnulbkgval
  endif
  endwhile
 close, v
 free_lun, v
w0=float(d)
w1=w0*transmisbkg                       ; tiny difference transmisbkg should be 1

FOR j=1,M DO BEGIN

FOR i=Ns, Nf DO BEGIN
        IF (i GT 9) THEN addnull='0' ELSE addnull='00'
        filei=strtrim(STRING(folder),2)+filenames(j-
1)+strtrim(STRING(addnull),2)+strtrim(STRING(i),2)+'.GQE'
        datfile=strtrim(STRING(datfolder),2)+filenames(j-
1)+strtrim(STRING(addnull),2)+strtrim(STRING(i),2)+'.dat'
 print,filei
 print,datfile
 openr,u,filei,/get_lun
 readu,u,h
 readu,u,d
 close, u
 free_lun,u

  openr,v,datfile,/get_lun
   calval=7.49168
   line= ""

   while (not eof (v)) do begin
   readf, v, line
   line= STRTRIM (line,2)       ; remove left whitespaces
   lengi=strlen(line)
```

```
    ; sucht nach "integral intensity I0/at prim.beamstop per sec"
    ionnulfind=strpos(line,'integral intensity I0 per sec')
    if (ionnulfind eq 0) then begin
     ionnul= strmid (line, 33)
     ionnulval=FLOAT(ionnul)
    endif

    iononefind=strpos(line,'integral intensity I1 per sec')
    if (iononefind eq 0) then begin
     ionone= strmid (line, 33)
     iononeval=FLOAT(ionnul)
    endif

    bsfind=strpos(line,'integral intensity at primary')
    if (bsfind eq 0) then begin
     bs= strmid (line, 50)
     bsval=FLOAT(bs)

     bsvalcal=bsval/calval
     transmis=bsvalcal/ionnulval
     ;print,transmis
     ;wait,1
    endif
    endwhile
   close, v
   free_lun, v

  data=float(d)
  corrdata=data/iononeval-w0/iononebkgval          ;formerly data-(w1*2)*transmis was used
  dvert=corrdata(275:275,0:511)
  dhor=corrdata(0:511,274:274)
  sumdvert=TOTAL(dvert)
  sumdhor=TOTAL(dhor)
  damageparam=sumdhor/sumdvert
 ;print,sumdvert
 ;print,sumdhor
 print,damageparam
  dvh[*,*, i-Ns]=damageparam
 ENDFOR

 dvhtot[*,*,N*(j-1):(N*j)-1]=dvh

 ENDFOR

 openw,uf,'ud6013res/dampud6013hv.dat',/get_lun
 printf,uf,dvhtot, FORMAT='(28(g0,1x))'  ;prints 28 data values horizontally and the next 28 below ...
 close,uf
 free_lun,uf

 END
```

The programme 'linfitdub.pro' reads the azimuthally integrated I(q)-data, corrects them for transmission and background, determines the logarithm and then applies a linear fit to obtain the power n with which the scattered intensity I falls with q and gives out this result in ascii for the whole scan region.

```
;determine power of Porod-law
h=STRARR(4,1) ;header of the .chi files
N=324                ; number of chi files, i changes from 1 to N per file
P=365                ; number of rows in the txtfile containing 2 columns: q(nm-1) and
Ns=1                 ; azimuthally integrated Intensity
Nf=324               ; number of bin files, i changes from 1 to N per file
elnum=365
trmisfactor=1.024          ;calibration factor for ion2 wrt ion1
bkgfactor=1.2              ;for steel and 20keV bkgd only 50s
ion2bkg=1.77E6       ;ion2bkg for files h04=1.77E6 b01=3.28E6 c00=2.78E6
d=fltarr(2,elnum)    ;variable containing raw saxs-data
e=fltarr(2,N)
f=fltarr(2,elnum)    ;variable containing ascii/txt-data
dvh=fltarr(1,1,N)
fitpar=fltarr(1,1,N)
filename='g03'                    ;first 3 letters characterizing the filename
chifolder='33760chi/'                   ;subdirectory or folder of saxs-data
txtfolder='33760mures/'           ;subdirectory or folder of ascii/txt-data
txtfilename='33760mug030405.txt'  ;ascii/txt-filename
txtfile=strtrim(STRING(txtfolder),2)+strtrim(STRING(txtfilename),2)
bkgfil='bkgfiles/bkgal20kevh04.chi'  ;corrected for 50->60s   ;background filename

 openr,ub,bkgfil,/get_lun          ;background file is read
 readf,ub,h,d
 close,ub
 free_lun,ub
 w1=float(d)/trmisfactor
 openr,ut,txtfile,/get_lun         ;txt-file for transmission correction is read
 readf,ut,e
 close,ut
 free_lun,ut
FOR i=Ns, Nf DO BEGIN

        IF (i GT 99) THEN BEGIN
                addnull='0'
        ENDIF ELSE BEGIN
                IF (i LT 10) THEN addnull='000' ELSE addnull='00'
        ENDELSE
        filei=strtrim(STRING(chifolder),2)+filename+strtrim(STRING(addnull),2)+strtrim(STRING(i),2)+'.chi'

 print,filei                       ;the chi-files containing I(q) (2 columns: I,q) are read
 openr,u,filei,/get_lun
 readf,u,h,f
 close,u
 free_lun,u

 ion2=e(1,i-1)                     ;the ion chamber 1 and 2 data are read from the txt-file
 ion1=e(0,i-1)                     ;and the transmission is determined for each scan point
;ion2 or ion2bkg=ion2 or ion2bkg)/trmisfactor, but trmisfactor can be omitted in normalization
 transmis=ion2/ion1                ;print,transmis, not used anymore
 Idata=f(1,*)                      ;the I(q)-data are separated into the two columns: I,q
 qdata=f(0,*)                      ;and I is corrected for background and transmission
 bkgdata=w1(1,*)
 corrIdata=Idata/ion2-bkgdata/(bkgfactor*ion2bkg)  ;correction for bkgd, transmission and I0-decay
```

```
FOR k=1,elnum DO BEGIN          ;'corrects' for negative data in tail end fluctuating region due to background
subtraction, should not effect tests over smaller ranges e.g. 40-175
                                        ; this was necessary to avoid NaN after taking log and losing info on
                                        points 2,6,9,12,15,17,23,38,53 file h02
        IF (corrIdata(k-1) LT 0) THEN BEGIN
        corrIdata(k-1)=-corrIdata(k-1)
        ENDIF
ENDFOR

 maxI=MAX(corrIdata,startch)
 logIdata=ALOG10(corrIdata)
 logqdata=ALOG10(qdata)
 Idatapart=logIdata(50:175)         ;number of channels/q-value range can be changed
 qdatapart=logqdata(50:175)         ;a meaningful part of the columns I and q is chosen

reslinfit=LINFIT(qdatapart,Idatapart,CHISQ=chi2,COVAR=covarm,MEASURE_ERRORS=deltavector,PROB
=probgt0p1,SIGMA=fitgood,YFIT=yfitvals)
 porodpower=reslinfit(1)
 offset=reslinfit(0)
 damageparam=-reslinfit(1)
 print,damageparam
 print,chi2
 dvh[*,*, i-Ns]=damageparam
 fitpar[*,*, i-Ns]=chi2

ENDFOR

openw,uf,'33760mures/frdimcornormg0350175.dat',/get_lun
printf,uf,dvh, FORMAT='(18(g0,1x))'  ;prints 18 data values horizontally and next 18 below ...
close,uf
free_lun,uf
openw,uf,'33760mures/chi2cornormg0350175.dat',/get_lun
printf,uf,fitpar, FORMAT='(18(g0,1x))'  ;prints 18 data values horizontally and next 18 below ...
close,uf
free_lun,uf

END
```

The program 'dampardub.pro' (DUBBLE-ESRF) reads in the raw image data, corrects them for transmission and background, then determines the ratio of the total intensity over a horizontal and vertical scan of the corrected image data and gives out this result in ascii for the whole scan region.

```
;determine the anisotropy parameter
h=lonarr (1281)
N=324                           ; number of bin files, i changes from 1 to N per file
P=324                           ; number of rows in the txtfile containing 2 columns: ion1, ion2
Ns=1
Nf=324                  ; number of bin files, i changes from 1 to N per file
trmisfactor=1.024
bkgfactor=1.2                   ;calibration factor for ion2 wrt ion1
ion2bkg=1.77E6          ;ion2bkg for files h04=1.77E6 (50s) b01=3.28E6 c00=2.78E6
d=uintarr(512,512)              ;variable containing raw saxs-data
e=fltarr(2,P)                   ;variable containing ascii/txt-data
dvh=fltarr(1,1,N)
dvert=fltarr(1,512)
dhor=fltarr(512,1)
filename='g03'                          ;first 3 lettres characterizing the filename
folder='33760mu/'                               ;subdirectory or folder of saxs-data
```

```
txtfolder='33760mures/'                    ;subdirectory or folder of ascii/txt-data
txtfilename='33760mug030405.txt'           ;ascii/txt-filename
txtfile=strtrim(STRING(txtfolder),2)+strtrim(STRING(txtfilename),2)
bkgfil='bkgfiles/bkg20kevh04.bin'          ;background filename, no correction for 50->60s
 openr,u,bkgfil,/get_lun
 readu,u,d
 BYTEORDER,d
 close,u
 free_lun,u
 w1=float(d)/trmisfactor

 openr,v,txtfile,/get_lun
 readf,v,e
 close, v
 free_lun, v

FOR i=Ns, Nf DO BEGIN

        IF (i GT 99) THEN BEGIN
                addnull='0'
        ENDIF ELSE BEGIN
                IF (i LT 10) THEN addnull='000' ELSE addnull='00'
        ENDELSE
        filei=strtrim(STRING(folder),2)+filename+strtrim(STRING(addnull),2)+strtrim(STRING(i),2)+'.bin'
        ;datfile=strtrim(STRING(datfolder),2)+filenames(j-
1)+strtrim(STRING(addnull),2)+strtrim(ST;RING(i),2)+'.dat'
 print,filei
;print,datfile
 openr,u,filei,/get_lun
 readu,u,d
 BYTEORDER,d
 close, u
 free_lun,u

 ion2=e(1,i-1)
 ion1=e(0,i-1)              ;ion2=ion2/trmisfactor, can be omitted in normalization
                            ;transmis=ion2/ion1, not used anymore
 data=float(d)
 corrdata=data/ion2-w1*bkgfactor/(bkgfactor*ion2bkg)
                            ;correcting/normalizing for transmission, bkgd and I0-decay
 dvert=corrdata(258:258,0:511)
 dhor=corrdata(0:511,253:253)
 sumdvert=TOTAL(dvert)
 sumdhor=TOTAL(dhor)
 damageparam=sumdhor/sumdvert          ;or the inverse

 print,damageparam
 dvh[*,*, i-Ns]=damageparam

ENDFOR

openw,uf,'33760mures/pg03cornormhv.dat',/get_lun
printf,uf,dvh, FORMAT='(18(g0,1x))'  ;prints 18 data values horizontally and next 18 below ...
close,uf
free_lun,uf

END
```